Questa Rock Pile Weathering and Stability Project

LITHOLOGIC ATLAS FOR THE QUESTA MINE, TAOS COUNTY, NEW MEXICO

Virginia T. McLemore, Dawn Sweeney, and Kelly Donahue

May 21, 2009

New Mexico Bureau of Geology and Mineral Resources

Open-file Report OF-516

Molycorp Task 1.2.2, B1.1

New Mexico Tech

EXECUTIVE SUMMARY

This report is one of a series of reports describing the effects of weathering on the long-term slope stability of the Questa rock piles. Descriptions of samples need to be consistent within this study as well as be consistent with other work being conducted by Chevron Mining, Inc. Thus, the purposes of this lithologic atlas are to:

- Familiarize workers with the lithologies that are most likely to appear in the Questa rock piles (i.e. the rocks that were mined from the open pit).
- Provide descriptions and photographs of these lithologies.
- Utilize the symbols that Chevron Mining, Inc. has identified as appropriate for naming the lithologies.
- Describe the alteration assemblages.
- Characterize the geochemistry of these altered lithologies.

This report includes descriptions and photographs of hand samples and thin sections of the different lithologies and alteration assemblages. Lithologies examined include andesite, quartz latite, rhyolite tuff (Amalia Tuff), aplite, granitic porphyry, miscellaneous dike, flows, volcaniclastic and tuffaceous rocks. Seven general types of hydrothermal alteration assemblages are found in the Red River-Rio Hondo and Questa districts and are found in the rock piles:

- Early and late propylitic (consisting of chlorite, calcite, pyrite, albite, epidote)
- Argillic and advanced argillic (consisting of chlorite, smectite, kaolinite, calcite, epidote, quartz, pyrite, clay minerals)
- Potassic (consisting of replacement of primary minerals by K-feldspar and potassium-bearing micas, illite, and sericite along with fluorite, quartz, and molybdenite)
- Quartz-sericite-pyrite (QSP), also is called phyllic, sericitic and silicic
- Magnetite veining
- Silicicfication (replacement by fine-grained quartz)
- Post-mineral carbonate-fluorite (locally with anhydrite)

Summary of current knowledge of composition of the overburden that went in the Questa rock piles:

- Chemically, the volcanic rocks in the Questa-Red River area are calc-alkaline, metaluminous to peraluminous igneous rocks.
- The rhyolite (Amalia Tuff) has more quartz and little to no epidote and chlorite compared to the andesite.
- The rhyolite (Amalia Tuff) typically has higher SiO_2, K_2O, Rb, Nb, less TiO_2, Al_2O_3, Fe_2O_3T, MgO, CaO, P_2O_5, and Sr than the andesite.
- Little, if any, unaltered rocks (i.e. primary magmatic) went into the Questa rock piles.
- The rock pile samples are a mixture of two or more rock types that were variably hydrothermally altered. GHN is a mixture of rhyolite (Amalia Tuff) and andesite.
- The rocks that went into the Questa rock piles were hydrothermally altered before mining, which resulted in large variations in mineralogical and chemical composition.
    - Amphiboles, pyroxenes, and feldspars were replaced by biotite and albite during alteration.

- Biotite, hornblende, pyroxenes were hydrothermally altered to chlorite, sericite, smectite, illite, and mixed layer clays (prophyllitic alteration).
- Feldspars show varying degrees of hydrothermal alteration to illite, kaolinite, smectite, quartz, mixed layer clays (QSP overprinting prophyllitic alteration).
- Many rocks were silicified, and this silicification was accompanied by the addition of 1-2 stages of pyrite, illite, calcite, and/or gypsum.

TABLE OF CONTENTS

EXECUTIVE SUMMARY 2
INTRODUCTION 10
Purpose 10
Acknowledgements 10
METHODS OF STUDY 11
GEOLOGIC HISTORY 12
QUESTA ROCK PILES 12
DESCRIPTION OF ALTERATION 14
Propylitic alteration (chlorite, ±epidote) 16
Argillic alteration 17
Potassic alteration 19
Phyllic or QSP alteration (Quartz-sericite-pyrite) 20
Silicification 20
Carbonate-fluorite and magnetite-hematite veins 21
MINERALOGY 21
Clay mineralogy 22
LITHOLOGIC DESCRIPTIONS 24
Felsic Intrusions 24
Goathill Porphyry 24
Christmas Tree porphyry or Hornblende feldspar porphyry 25
Plagioclase (biotite) aplite porphyry 28
Granite porphyry 29
Amalia Tuff 29
Latir Volcanic Rocks 34
Coarse-grained porphyritic andesite 35
Fine-grained porphyritic andesite 37
Fine-grained andesite 39
Quartz latite 39
Fine-grained, porphyritic andesite 40
Biotitized andesite 41
Andesite breccia 42
Volcaniclastic rocks 44
CHEMICAL CHARACTERIZATION OF THE LITHOLOGIES AND ALTERATION ASSEMBLAGES AT QUESTA 45
PARAGENESIS OF HYDROTHERMAL ALTERATION 50
SUMMARY 53
REFERENCES 54
APPENDIX 1. COMPOSITION OF VOLCANIC AND INTRUSIVE ROCKS IN THE QUESTA-RED RIVER AREA 59

FIGURES

FIGURE 1. Location of the Questa rock piles and other mine features, including location of trenches constructed in Goathill North (GHN) rock pile 13

FIGURE 2. Cross section showing schematic spatial distributions of lithologies, alteration assemblages, and alteration scars in the Red River valley (taken from Ludington et al., 2005, which is modified from Martineau et al., 1977)..... 18
FIGURE 3. Propyllitic alteration as indicated by green chlorite (chl) and brown feldspar (kspar) minerals in sample GMG-PIT-0013 in plane polarized light; field of view is approximately 1.8 mm..... 19
FIGURE 4. Backscattered electron microprobe image showing argillic alteration where clay minerals replacing feldspar phenocrysts (kspar) in sample PIT-KMD-0007 19
FIGURE 5. Sample PIT-LFG-0001 shows moderate QSP alteration under crossed polarized light; field of view is approximately 1.8 mm. The feldspar phenocryst (kspar) is well-defined and the groundmass is replaced by quartz and sericite.... 20
FIGURE 6. Sample PIT-KMD-0007 showing moderate to strong QSP alteration. The feldspar (kspar) phenocryst are replaced by quartz and sericite and the grain boundaries are poorly defined both in plain polarized light and under crossed polarized light; field of view is approximately 1.8 mm..... 21
FIGURE 7. a) The XRD results of drill-core clay analyses of propllytically altered andesite samples, b) the XRD results of andesite and rhyolite QSP-altered core samples and c) andesite and rhyolite drill core samples with evidence of over-printing hydrothermal alteration assemblages. I = illite, K = kaolinite, C = chlorite, S = smectite, Gy = gypsum..... 23
FIGURE 8. Sample ROC-VTM-G005 showing typical propylitic texture of the cream-colored Goathill Porphyry..... 24
FIGURE 9. Sample ROC-VTM-G011 is QSP-altered Goathill Porphyry. Note the holes caused by loss of quartz phenocrysts. This rock in a weathered state would be stained yellow 24
FIGURE 10. (A) Sample ROC-VTM-G007 is coarse-grained, cream-colored, phenocryst-rich Christmas Tree Porphyry (Thfp) with black hornblende, clear quartz, and cream feldspar phenocrysts. (B) Sample PIT-KMD-0001 showing hand sample of cream-colored, porphyritic, Christmas Tree Porphyry. 26
FIGURE 11. Thin section of sample PIT-KMD-0001 showing Christmas Tree porphyry, consisting of quartz, feldspar, calcite, clays and trace amounts of pyrite, magnetite and biotite. Magnification is 5 times and field of view is 1.8 mm. 26
FIGURE 12. Sample ROC-VTM-G008 is coarse-grained, cream-colored, phenocryst-rich Christmas Tree porphyry intruded by a small cream-colored aplite dike..... 26
FIGURE 13. (A) Sample ROC-VTM-G027 is QSP-altered aplite porphyry with trace of pyrite. (B) Sample PIT-VCV-0028 is QSP-altered aplite porphyry with fresh disseminated pyrite 27
FIGURE 14. Thin section photographs of sample PIT-VCV-0028 showing QSP-altered aplite, under plane polarized light (A) and with crossed polarized light (B), 5 times magnification and a field of view of approximately 1.8 mm. Illite has replaced the feldspar phenocryst..... 27
FIGURE 15. Sample ROC-VTM-G026 is fine-grained (aplitic) phase of the QSP-altered Christmas Tree porphyry consisting of very small quartz, feldspar, and hornblende phenocrysts and 5% disseminated pyrite 27

FIGURE 16. (A) Sample ROC-VTM-G010 is pink, plagioclase aplite porphyry to porphyritic aplite with quartz, feldspar, and biotite phenocrysts. (B) Sample ROC-MZQ-0006 is peach-colored, fine-grained, plagioclase aplite..... 28
FIGURE 17. Thin section photograph of sample ROC-MZQ-0006 showing aplite with quartz, feldspar and some biotite under normal polarized light (A) and crossed polarized light (B). Magnification is 5 times and field of view is 1.8 mm..... 28
FIGURE 18. (A) Sample ROC-VTM-G012 is granite porphyry from the underground deposit. (B) Sample PIT-VCV-0016 is granite porphyry with pink feldspars, quartz, and greenish-black micas..... 29
FIGURE 19. Thin section photos of sample PIT-VCV-0016 under normal polarized light (A) and crossed polarized light (B) with quartz, feldspars, and micas, 5 times magnification and field of view of approximately 1.8 mm..... 29
FIGURE 20. (A) Sample ROC-VTM-G001 is welded Amalia Tuff showing flow banding formed by black obsidian (pumice) foliation. (B) Sample PIT-VCV-0002 is hand sample of Amalia Tuff with flow banding and remnant obsidian and pumice fragments..... 30
FIGURE 21. Thin section photographs of sample PIT-VCV-0002 under normal plane polarized light (A) and crossed polarized light (B) showing flow banding around quartz phenocrysts, 5 times magnification and field of view of approximately 1.8 mm..... 31
FIGURE 22. (A) Sample ROC-VTM-G002 is welded Amalia Tuff showing flow banding formed by black obsidian (pumice) foliation (Topt). (B) Sample PIT-VTM-0006 is slightly QSP-altered drill core of Amalia Tuff with flow banding..... 31
FIGURE 23. Thin section photographs of sample PIT-VTM-0006 under normal plane polarized light (A) and crossed polarized light (B) showing flow banding surrounding feldspar phenocrysts, 5 times magnification and field of view of approximately 1.8 mm..... 31
FIGURE 24. Sample ROC-VTM-G003 is flow-banded rhyolite tuff (Amalia Tuff) showing eutaxitic foliation. Misnamed as pit porphyry..... 32
FIGURE 25. (A) Sample ROC-VTM-G019 is slightly porphyritic rhyolite with foliation. Small pyrite cubes disseminated in rock. Called pit porphyry, but is actually Amalia Tuff. (B) Sample PIT-VCV-0006 is hand sample showing porphyritic texture and remnant flow banding..... 32
FIGURE 26. Thin section photographs of sample PIT-VCV-0006 under normal plane polarized light (A) and crossed polarized light (B) showing flow banding around quartz and feldspar phenocrysts, 5 times magnification and field of view of approximately 1.8 mm..... 32
FIGURE 27. Sample ROC-VTM-G004 is flow-banded rhyolite tuff, Amalia Tuff, typical of outflow units..... 33
FIGURE 28. Thin section photographs of sample PIT-LFG-0011 under normal plane polarized light (A) and crossed polarized light (B) showing flow banding around quartz phenocrysts, 5 times magnification and field of view of approximately 1.8 mm..... 33
FIGURE 29. Sample ROC-VTM-G030 is QSP-altered Amalia Tuff with remnant flow banding and 1% pyrite..... 33

FIGURE 30. Thin section photographs of sample ROC-MZQ-0004, Amalia Tuff, under normal plane polarized light (A) and crossed polarized light (B) showing quartz and sanidine. Magnification is 5 times and field of view is 1.8 mm 34
FIGURE 31. Sample ROC-VTM-G020 showing two phases of Amalia Tuff, pumice flow banding and crystal rich. Note crystals are broken 34
FIGURE 32. Sample ROC-VTM-G009 is mudflow facies of the Amalia Tuff (Trt), typically found at the rhyolite flow, with an andesite fragment 34
FIGURE 33. (A) Sample ROC-VTM-G015 is relatively fresh andesite of the Latir volcanics sequence. (B) Sample PIT-KMD-0009 is porphyritic andesite with some propylitic alteration 35
FIGURE 34. Thin section photographs of sample PIT-KMD-0009, andesite under normal plane polarized light (A) and crossed polarized light (B) showing propylitically-altered feldspars (cream colored) and chlorite (green) minerals. Feldspars show replacement by illite (brown). Magnification is 5 times and field of view is approximately 1.8 mm 35
FIGURE 35. (A) Sample ROC-VTM-G017 is yellow and reddish stained quartz latite of the Latir volcanics with phenocrysts. (B) Sample GMG-PIT-0015 is hydrothermally-altered porphyritic andesite sample 36
FIGURE 36. Thin section photographs of sample GMG-PIT-0015, andesite under normal plane polarized light (A) and crossed polarized light (B) showing a highly altered relic hornblende crystal with pyrite inclusions in a fine-grained groundmass, 5 times magnification and field of view of approximately 1.8 mm..... 36
FIGURE 37. Sample ROC-VTM-G016 is light gray porphyritic, crystal-rich andesite of the Latir volcanics with feldspar, biotite, and hornblende phenocrysts..... 37
FIGURE 38. (A) Sample ROC-VTM-G021 is greenish gray, finely porphyritic andesite of the Latir volcanics with epidote alteration. (B) Sample PIT-VCV-0009 is propylitically-altered porphyritic andesite with disseminated pyrite..... 38
FIGURE 39. Thin section of sample PIT-VCV-0009, andesite, under normal plane polarized light (A) and crossed polarized light (B) showing quartz, feldspar, and pyrite grains in a fine-grained groundmass. Magnification is 5 times and field of view is approximately 1.8 mm. 38
FIGURE 40. (A) Sample ROC-VTM-G025 shows a vein of quartz-pyrite-sericite (QSP alteration) cutting andesite of the Latir volcanics. (B) Sample PIT-KMD-0007 is QSP-hydrothermally-altered andesite with finely disseminated pyrite and quartz-molybdenum-pyrite veining..... 38
FIGURE 41. Thin section photographs of sample PIT-KMD-0007, andesite, under normal plane polarized light (A) and crossed polarized light (B) showing highly altered feldspar phenocrysts replaced by illite and with chlorite (green) and other clay minerals. Magnification is 5 times and field of view is approximately 1.8 mm 39
FIGURE 42. Sample ROC-VTM-G023 is greenish-gray, propylitic-altered, fine-grained andesite of the Latir volcanics. Pyrite-filled fractures cut the andesite 39
FIGURE 43. (A) Sample ROC-VTM-G013 is gray quartz latite flow of the Latir volcanics with feldspar, quartz, hornblende phenocrysts. (B) Sample GMG-PIT-0009 is white-gray hydrothermal-altered quartz latite porphyry with pink and white feldspar phenocrysts..... 40

FIGURE 44. Thin section photographs of sample GMG-PIT-0009, andesite, under normal plane polarized light (A) and crossed polarized light (B) showing quartz and feldspar phenocrysts with a hydrothermally altered mica grain, now chlorite, in a fine-grained hydrothermally altered groundmass. Magnification is 5 times and field of view is approximately 1.8 mm 40
FIGURE 45. Sample ROC-VTM-G022 is fine-grained, porphyritic andesite of the Latir volcanics. Porphyritic texture with small phenocrysts of feldspar and disseminated pyrite 41
FIGURE 46. Sample ROC-VTM-G031 is fine-grained, porphyritic andesite of the Latir volcanics showing phyllic alteration overprinted by QSP alteration..... 41
FIGURE 47. Sample ROC-VTM-G014 is fine-grained black andesite of the Latir volcanics containing pyrite and showing biotitization..... 42
FIGURE 48. (A) Sample ROC-VTM-G029 is andesite breccia of the Latir volcanics, locally called watermelon breccia. (B) Sample MIN-VTM-0001 is hand sample of watermelon breccia 42
FIGURE 49. Thin section photographs of sample MIN-VTM-0001, andesite, under normal plane polarized light (A) and crossed polarized light (B) showing chlorite (green to brown) and altered feldspars replaced by illite (cream colored). Magnification is 5 times and field of view is approximately 1.8 mm 43
FIGURE 50. Sample ROC-VTM-G028 is andesite breccia of the Latir volcanics 43
FIGURE 51. Sample ROC-VTM-G024 is greenish-gray to purplish-gray andesite breccia of the Latir volcanics with propylitic alteration. Pyrite mineralized clasts are outlined 44
FIGURE 52. Photograph of sample GHR-VWL-0006-T002 is a hydrothermally altered, matrix-supported sandstone 44
FIGURE 53. Photograph of sample GHR-VWL-00011-T002 is a hydrothermally altered, fine-grained sandstone 45
FIGURE 54. Lithogeochemical classification plots of relatively unweathered volcanic and intrusive rocks (including various hydrothermally-altered rocks) for the Questa-Red River area. Chemical analyses are in the Appendix 1. ANK=Al_2O_3+Na_2O+K_2O. ACNK=Al_2O_3+CaO+ Na_2O+K_2O 48
FIGURE 55. Scatter plots of selected elements and SiO_2 of relatively unweathered volcanic and intrusive rocks (including various hydrothermally-altered rocks) for the Questa-Red River area. Chemical analyses are in Appendix 1..... 49
FIGURE 56. Graphs of relatively unweathered volcanic and intrusive rocks (including various hydrothermally-altered rocks) using alteration filter diagrams showing unaltered and hydrothermally altered fields (after Wilt, 1995; Keith and Swan, 1996; McLemore et al., 1999). Chemical analyses are in the project database. Major element oxides are in weight percent and trace elements are in parts per million (ppm). 50
FIGURE 57. General paragenesis of mineralization and alteration (from Molling, 1968). MHBx event is the main mineralizing event, which is described in detail by Ross et al. (2002) in Table 9 and Figure 58..... 51
FIGURE 58. Paragenesis of the Questa breccia ore deposit (from Ross et al., 2002). A-E represents the different breccia facies..... 52

FIGURE 59. Paragenesis of the Questa mineral deposit and alteration (from Meyer and Leonardson, 1990) 53

TABLES

TABLE 1. Summary of geologic history of the Questa area (Bauer et al., 2004; Ludington et al., 2005; Samuels, 2008; Zimmerer, 2008) 13
TABLE 2. Estimates of volume of each lithology mined from the open pit deposit. 14
TABLE 3. Relative stabilities, approximate concentrations, and compositions of minerals found in Questa rock pile deposits (NM Tech electron microprobe results in bold, other elements by Molling, 1989; Shum, 1999; Piché and Jébrak, 2004; Plumlee et al., 2005). 21
TABLE 4. Summary descriptions of felsic intrusions. Sample locations are given in the UTM column (zone 13). na indicates the UTM coordinates are not available for the sample (samples are from the Chevron rock collection)..... 25
TABLE 5. Summary descriptions of Amalia Tuff. na indicates the UTM coordinates are not available for the sample 30
TABLE 6. Summary descriptions of Latir volcanic lithologies. No locations of samples are available 36
TABLE 7. Average range in modal mineralogical compositions in weight percent of relatively unweathered major volcanic and intrusive rocks at the Questa mine (Lipman and Read, 1989; Molling, 1989; Meyer, 1991; and petrographic analyses by E.H. Phillps, D. Sweeney, V.T. McLemore). 45
TABLE 8. Chemical composition of relatively unweathered volcanic and intrusive rocks (including various hydrothermally-altered rocks) from the Questa-Red River area (from Dillet and Czamanske, 1987; Lipman, 1988; Johnson et al., 1989; P. Lipman, written communication, 2007, and project data). Major oxides in percent and trace elements in parts per million (ppm). 46
TABLE 9. Comparison of paragenesis of the vein and breccia deposits by different workers. q=quartz, b=biotite, K-K-feldspar, mo=molybdenite, f=fluorite, ru=rutile, py=pyrite, cc=calcite, cp=chalcopyrite, sp=sphalerite, gn=galena, rh=rhodocrosite, gy=gypsum, mh=malachite, lm=limonite, s=sericite. Ross et al. (2002) describes the paragenesis only of the main MHBx mineralizing event. ... 50

INTRODUCTION

Purpose

The Chevron Mining Inc. (formerly Molycorp, Inc.) Questa molybdenum mine is located on the western slope of the Taos Range of the Sangre de Cristo Mountains of the Southern Rocky Mountains near the edge of the Rio Grande rift in north-central New Mexico. The mine is on southward facing slopes and is bounded on the south by Red River (elevation of approximately 7500 ft) and on the north by the mountain divides (elevation approximately 10,750 ft). During the period of open-pit mining (1969-1982) at the Questa mine, approximately 350 million tons of overburden rock was removed and deposited onto mountain slopes and into tributary valleys forming nine rock piles surrounding the open pit. These are some of the highest rock piles in the United States. Since the rock piles were emplaced, a number of shallow-seated failures, or slumps, have occurred at Questa and a foundation failure occurred at Goathill North rock pile that resulted in sliding of the rock pile (Norwest Corporation, 2004). The purpose of the Questa Rock Pile Weathering and Stability Project (QRPWASP) is to determine what changes will occur in the rock piles over long periods of time (100 and 1000 years) due to weathering (both physical and chemical changes) and the effect of these changes on overall rock-pile stability.

This report is one of a series of reports describing the effects of weathering on the long-term slope stability of the Questa rock piles. Descriptions of samples need to be consistent within this study as well as be consistent with other work being conducted by Chevron Mining, Inc. Thus, the purposes of this lithologic atlas are to:

- Familiarize workers with the lithologies that are most likely to appear in the Questa rock piles (i.e. the rocks that were mined from the open pit).
- Provide descriptions and photographs of these lithologies.
- Describe the alteration assemblages.
- Characterize the geochemistry of these altered lithologies.

This report includes descriptions and photographs of hand samples and thin sections of the different lithologies and alteration assemblages. Note that scales of the photographs are in centimeters. Higher resolution photographs are available as part of the project database. The photographs are labeled by their sample numbers and location data can be found in the project database. Characterization of the alteration scar areas are in a separate report (Graf, 2008).

Acknowledgements

This project was funded by Chevron Mining, Inc. (formerly Molycorp, Inc.) and the New Mexico Bureau of Geology and Mineral Resources (NMBGMR), a division of New Mexico Institute of Mining and Technology. We would like to thank the professional staff and students of the large multi-disciplinary field team for their assistance in mapping, sampling, and laboratory analyses. This report could not have been written without the years of work by Chevron Mining, Inc. geologists, especially Bruce Walker, and correlation efforts by Cori Hoag and her team from SRK and mapping by Mark Osterburg. Whole rock geochemical analysis was by Washington State University. Peter Lipman provided some of the chemical analyses used in this report. Nelia Dunbar, Bruce Walker, Soloman Ampim, Ariel Dickins and Jack Hamilton reviewed earlier versions of this report. This report is part of an on-going study of the

environmental effects of the mineral resources of New Mexico at NMBGMR, Peter Scholle, Director and State Geologist.

METHODS OF STUDY

This study includes a review of the literature, field observations and sampling, and petrographic, mineralogical and chemical characterization of samples of various lithologies in the Questa-Red River area. Several different types of samples were collected:

- Outcrop samples of unweathered (or least weathered) igneous rocks representative of the mined rock (overburden) (includes all predominant lithologies and alteration assemblages at various hydrothermal alteration and weathering intensities)
    - andesite
    - quartz latite
    - rhyolite tuff (Amalia Tuff)
    - aplite, granitic porphyry
    - miscellaneous dike, flow, and tuffaceous rocks
    - alteration scars
- Samples of the vein material within altered host rocks (typically veins are <2 cm)
    - quartz-molybdenite-pyrite (orthoclase flooding, biotite)
    - quartz-sericite-pyrite of rhyolite porphyry dikes
    - quartz-fluorite-sericite-pyrite-base metal sulfides (halo above mineral deposits)
    - calcite-gypsum/anhydrite
- Weathering profiles of colluvium/weathered bedrock and alteration scars
- Sections of drill-core samples of the mined rock (overburden) and ore deposit before mining.

Different sampling strategies were employed based upon the purpose of each sampling task. Typically, at each site, a select, grab, or bulk sample of rock or soil material was collected for petrographic study and geochemical and geotechnical analyses. A hand specimen was collected from some sites for thin section analysis. The samples for this report consisted of grab samples of two or more pieces of outcrop or drill core samples (typically 3-8 cm in diameter). These samples are more homogeneous than rock-pile samples in that they are composed of one lithology and alteration assemblage, whereas the rock-pile material typically consists of multiple lithologies and/or alteration assemblages. A portion of the collected sample was crushed and pulverized for geochemical analysis. Thin sections were made of another piece of selected rock samples for petrographic analysis (including estimated modal mineralogical analysis). Some of the samples examined were obtained from the Chevron rock collection and only hand specimen descriptions of these rocks were performed. Additional mineralogical and chemical analyses of rock types were obtained from the literature and Peter Lipman (USGS). More detailed petrographic data are in the project database.

Samples were petrographically analyzed using a binocular microscope. Petrographic analysis included identification of minerals, lithologies and alteration types (propyllitic, argillic, or quartz-sericite-pyrite (QSP) alteration). Propyllitic alteration is

characterized by the presence of chlorite, epidote, calcite and pyrite. Argillic or clay alteration is characterized by the addition of clay minerals, especially chlorite and smectite. QSP alteration is characterized by the abundant presence of quartz and sericite (illite). Pyrite is found in both propyllitic and QSP alteration types. Amalia Tuff was identified by the presence of fiamme (flattened pumice) and relatively small phenocryst size. Intrusive aplite samples were identified using crystalline textures, i.e. quartz in andesite and Amalia Tuff look different than quartz in intrusive aplite samples. Lithology and mineral abundances were visually estimated with standardized charts. Alteration intensity was also estimated.

Mineralogical data is obtained from several different techniques, including:

- Petrographic analysis of a bulk grab sub-sample using a binocular microscope (van der Plas and Tobi, 1965)
- Petrographic analysis of thin sections of the rock fragments using a petrographic microscope (including both transmitted- and reflected-light microscopy; van der Plas and Tobi, 1965; Delvigne, 1998)
- Electron microprobe analysis of both the fine-grained soil matrix and the rock fragments
- Clay mineral determination of a bulk sample split using clay separation techniques and X-ray diffraction analysis (Moore and Reyolds, 1989; Hall, 2004)
- Other methods of determining mineralogy (spectral analysis, X-ray diffraction, fizz test).

The bulk quantitative mineralogy was determined using a modified ModAn technique along with petrographic observations (including an estimated modal analysis), electron microprobe analysis, clay mineral analysis, and the whole-rock chemistry of the sample, as described by McLemore et al. (2009b). ModAn is a modeling program that uses whole-rock chemical and petrographic analyses to determine a normative quantitative mineralogy of the sample (Paktunc, 1999, 2001).

GEOLOGIC HISTORY

The geology and mining history of the Questa-Red River area is complex, described by others (Carpenter, 1968; Clark, 1968; Reed et al., 1983; Lipman, 1988; Meyer and Leonardson, 1990; Czamanske et al., 1990; Roberts et al., 1990; Ludington et al., 2005), and summarized in McLemore (2009) and Table 1. Lithologies likewise are diverse, including granitic and gabbroic intrusive rocks and rhyolitic and andesitic volcanic rocks.

QUESTA ROCK PILES

Approximately 135 million lbs of molybdenum were produced from the open-pit deposit (1969-1981) that resulted in approximately 350 million tons of overburden rock material deposited onto mountain slopes and into tributary valleys forming the nine rock piles and 50 million tons of tailings stored in the Guadalupe Mountain tailings facility at Questa (Fig.1). The current mine is an underground, molybdenum disulfide (“moly”) mine that uses a block-caving mining method to extract ore.

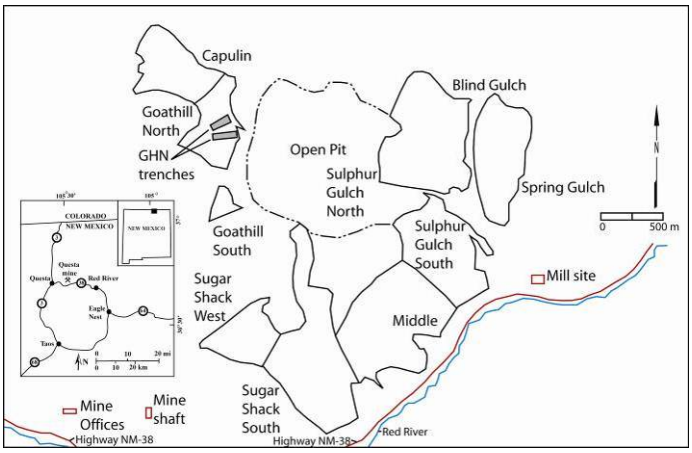

FIGURE 1. Location of the Questa rock piles and other mine features, including location of trenches constructed in Goathill North (GHN) rock pile.

TABLE 1. Summary of geologic history of the Questa area (Bauer et al., 2004; Ludington et al., 2005; Samuels, 2008; Zimmerer, 2008).

Approximate age	Event	Event
2 Ma-present	Pediment and stream deposits	
4.5 Ma-present	Beginning of alteration of scars	
2.34-5.88 Ma	Taos Plateau volcanic field	
1-16.4 Ma	Santa Fe Group	Miocene lavas
5 Ma to present	Slow extension, basin subsidence	
18.6-5 Ma	Rapid extension of Rio Grande rift	
16.5-22.9	Postcaldera magmatism, southern margin	
24.7-22 Ma	Resurgent plutonism, postcaldera volcanism, southern caldera margin plutonism and Mo mineralization (Latir Peak volcanic field)	Slow extension of Rio Grande rift
25.2 Ma	Amalia Tuff (Questa caldera collapse)	peralkaline rhyolite dikes
25.2-28.3 Ma	Precaldera volcanism (Latir Peak volcanic field)	sedimentary rocks
28.5-33.7 Ma	Early regional extension Rio Grande rift	Transition from crustal shortening to extension
33.7-65 Ma	Laramide orogeny	
1610-1752 Ma	Precambrian rocks	

The amount of the various lithologies that were mined from the open-pit deposit was calculated from Chevron data. The tailings or ore were not subtracted out. The procedure is summarized below:

1. Calculate areas for each lithology within the open pit as mapped on cross sections provided by SRK, using either rectangles or triangles.

2. Calculate a volume by multiplying each area by 200 ft (the distance between cross sections). This assumes that each lithology is a simple box.
3. Calculate total volume mined and divide each lithology to get a percentage of the lithology mined.

These estimated results are summarized by lithology in Table 2.

TABLE 2. Estimates of volume of each lithology mined from the open pit deposit. Description of the lithologies follows in the next section. The relative estimate of strength is based upon analyses of fractures and perceived integrity of the rock, which is dependent upon mineralogy (i.e. the more quartz in the rock, the stronger the rock, the more illite and chlorite, the weaker the rock). Symbols in parentheses are from Lipman and Reed (1989). QSP is quartz-sericite-pyrite hydrothermal alteration.

Symbol	Lithology	Volume (percent)	Relative estimate of strength (1 strong, 3 weak)	Comments
Tdqpt-Trt (Trt, Trtl)	Amalia Tuff	10	1	Mostly QSP altered, no ore
Tanbx	Andesite breccia (includes latite, quartz latite and volcaniclastic rocks)	14	3 2	50% QSP, 50% propylitic, no ore
Tanfp (Ta)	Fine-grained andesite (includes latite, quartz latite)	46	3 2	50% QSP, 50% propylitic, some ore
Thfp	Christmas Tree porphyry	8	2	QSP altered, no ore, pyrite rich
Tpap (Tgy)	Aplite (includes granite and rhyolite dikes)	22	1	Most of ore from this unit
TOTAL		100		

Records were not kept detailing the construction of the rock piles. However, URS Corporation (2003) presents a summary of their construction as interpreted from dated air photographs. The development of the Questa open pit began with excavations along the west side of the pit and development continued progressively southeast along Sulphur Gulch. The top layers of the volcanic series, mainly the rhyolite (Amalia Tuff) and andesites (flows and porphyry units), located along the west side of the pit were mined first and placed in the rock piles. A portion of the large natural alteration scar (which has relatively high pyrite concentrations) located on the west and northwest side of the open pit (Questa Pit Scar in Sulphur Gulch) was mined early in the development of the open pit. Aplite and granite were mined from the lower portion of the open pit and the aplite overlies the black andesite. A wrap-around berm of aplite provided a shallow cover over the mixed volcanics unit over the lowest lift of the southern mine rock piles.

DESCRIPTION OF ALTERATION

Alteration is a general term describing the changes in mineralogy, texture, and chemistry of a rock as a result of a change in the physical, thermal, and chemical environment in the presence of water, steam, or gas, including those changes produced by weathering (Henley and Ellis, 1983; Reed, 1997; Neuendorf et al., 2005; Ludington et al., 2005). The nature of the alteration depends upon (Browne, 1978; Henley and Ellis, 1983; Ludington et al., 2005):

- Temperature and pressure (including amount of overburden or depth) at the alteration site
- Composition of the parent rock
- Composition of the altering (invading) fluids
- Permeability of the parent rock
- Duration and intensity of the alteration process (i.e. time)
- Distance from the alteration source, resulting in alteration zoning.

Alteration includes hypogene or hydrothermal (primary), supergene (secondary), and weathering alteration. *Hypogene alteration* occurred below the surface during the formation of the ore body by upwelling (ascending), hydrothermal or warm to hot fluids (Neuendorf et al., 2005). *Supergene alteration* is the natural weathering, before mining, of the ore body, at low temperatures near the Earth's surface by descending fluids (Neuendorf et al., 2005). *Weathering* is the set of physical and chemical changes, up to and including disintegration of rock by physical, chemical, and/or biological processes occurring at or near the earth's surface (e.g., in the vadose zone within approximately 100 m of ground surface at temperatures less than or equal to approximately 70°C) that result in reductions of grain size, changes in cohesion or cementation, and change in mineralogical composition (modified from Neuendorf et al., 2005). General discussions of hydrothermal alteration associated with Climax-type porphyry molybdenum deposits are by Westra and Keith (1981), Mutschler et al. (1981), Ludington (1986), Carten et al. (1993), and Ludington et al. (1995, 2005). This report describes the hypogene (hydrothermal) and supergene alteration. The effects of weathering after being emplaced in the rock piles are described in McLemore et al. (2006a, b, 2008a, b).

The hydrothermal alteration at Questa is similar to most Climax-type porphyry molybdenum systems and exhibits a distinctive district alteration zoning (Fig. 2; Martineau et al., 1977; Loucks et al., 1977; Molling, 1989; Meyer and Leonardson, 1990; Ross et al., 2002; Ludington et al., 2005). The mined overburden material that went into the rock piles was mostly from the upper portions of the hydrothermally altered system. Seven general types of hydrothermal alteration assemblages are found in the Red River-Rio Hondo and Questa districts and are found in the rock piles (Fig. 2; Martineau et al., 1977; Molling, 1989, Meyer, 1991; Reed, 1997):

- Early and late propylitic (consisting of chlorite, calcite, pyrite, albite, epidote)
- Argillic and advanced argillic (consisting of chlorite, smectite, kaolinite, calcite, epidote, quartz, pyrite, clay minerals)
- Potassic (consisting of replacement of primary minerals by K-feldspar and potassium-bearing micas, illite, and sericite along with fluorite, quartz, and molybdenite)
- Quartz-sericite-pyrite (QSP), also is called phyllic, sericitic and silicic
- Magnetite veining
- Silicicfication (replacement by fine-grained quartz)
- Post-mineral carbonate-fluorite (locally with anhydrite).

The manner in which these alterations express themselves mineralogically and chemically depends on:

- The original rock types
- The paleo-hydrology that distributed the alteration solutions

- Subsequent geologic history
- Intensity of molybdenum mineralization.

Supergene alteration is commonly superimposed on the hypogene alteration, especially in near-surface rocks mined early in the history of Questa. In some places, supergene weathering along open fracture systems can extend to considerable depths. Weathering is superimposed on both the hypogene and supergene alteration.

Regional fracturing of the pre-mined rock occurred during igneous intrusion and hydrothermal alteration and formed jointed rocks with a few distinctive patterns such as orthogonal, oblique orthogonal, and conjugate joint sets (Caine, 2003, 2006; Ludington et al., 2005). Three types of fault zones are present and include partially silicified, low- and high-angle faults with well-developed damage zones and clay-rich cores and high-angle, unsilicified open faults (Caine, 2006). These faults and fractures not only provide pathways for modern fluids (Caine, 2006), but also provide for angular rock fragments when the material is blasted. These angular rock fragments when found in the rock pile provide for stronger material (McLemore et al., 2009a).

Propylitic alteration (chlorite, ±epidote)

Propylitic alteration, in part, spatially overlaps and, in part, occurs peripherally to QSP alteration. It typically forms at low temperatures, 200-350ºC (Reed, 1997). This mineral assemblage consists of essential chlorite (producing the green color), epidote, albite, pyrite, quartz, carbonate minerals, and a variety of additional minerals depending upon host-rock lithology, temperature, and composition of the fluids, including zeolites, adularia, sericite/illite, smectite, kaolinite, etc. Propylitically altered rocks are typically green to green-gray in color as a result of the presence of chlorite and epidote (Fig. 3). Hematitization producing a brown to red-brown color masking the green color also is common. Propylitic alteration occurred in two phases in the Questa-Red River area:

- Early stage, overlaping QSP alteration
- Late, district-wide stage followed by QSP alteration.

It is difficult to distinguish between these two stages (Ludington et al., 2005). Propylitic alteration is best developed in andesites, latites, volcanic breccias, and volcaniclastic rocks and less developed in the granitic porphyries and rhyolite (Amalia Tuff), because the granitic and rhyolitic rocks have less mafic minerals containing Ca, Mg, Mn, and Fe required to form chlorite and epidote.

The groundmass is replaced by quartz, calcite, smectite, kaolinite, and chlorite; feldspar phenocrysts are partially or completely replaced by quartz, chlorite, albite, and calcite. Episodic periods of alteration probably occurred as evidenced by overlapping veinlets and replacement textures. Thin veinlets of quartz-pyrite or calcite, less than a millimeter wide, cut across chloritized andesite, but are subsequently offset by younger veinlets of calcite. Epidote and chlorite locally replace plagioclase. Quartz-pyrite and pyrite veinlets are common along fractures within the andesite. Disseminated pyrite occurs in the andesite and pyrite locally replaces hornblende and olivine grains in the andesite. These different forms and occurrences of pyrite suggest several stages of pyrite occurred.

Argillic alteration

Argillic or clay alteration consists of kaolinite, smectite (montmorillonite clays), chlorite, epidote, and sericite and overlaps the other types of hydrothermal alteration. Chlorite has replaced mafic minerals and the groundmass within the andesite. Disseminated pyrite is locally pervasive in the andesite. Locally, chlorite and epidote veinlets formed along fractures. Calcite occurs as thin veins and also replaces feldspar crystals. Sericite also replaces K-feldspar phenocrysts (Fig. 4). Advanced argillic alteration consists of kaolinite, quartz, alunite, jarosite, pyrophyllite, and other aluminosilicate minerals and is found in the alteration scars and along some faults in the mine area. Argillic alteration is best developed in andesites, latites, volcanic breccias, and volcaniclastic rocks, but is common in the granitic porphyries and rhyolite (Amalia Tuff), because the available minerals can alter to clay minerals during hydrothermal alteration.

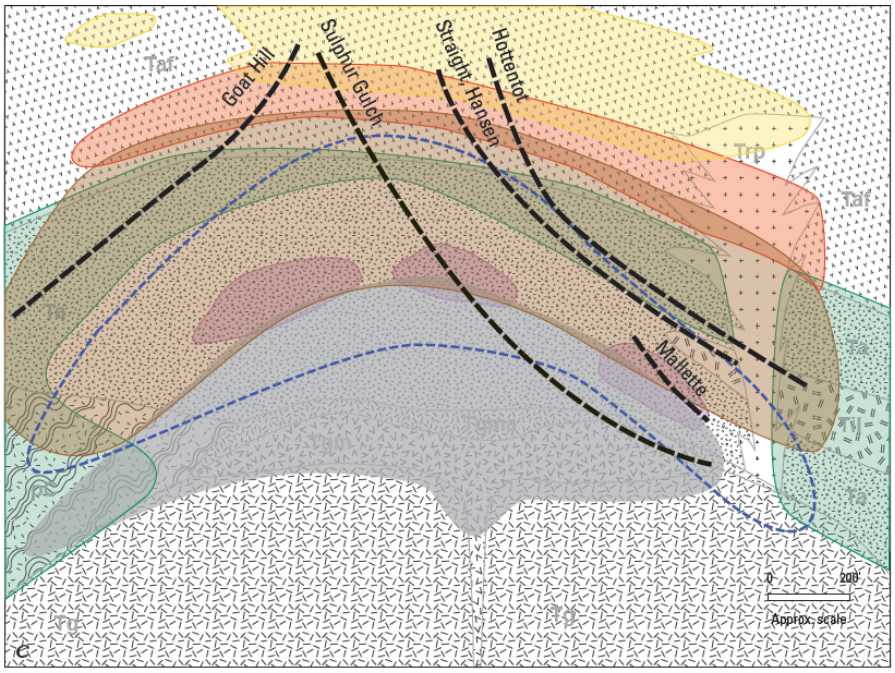

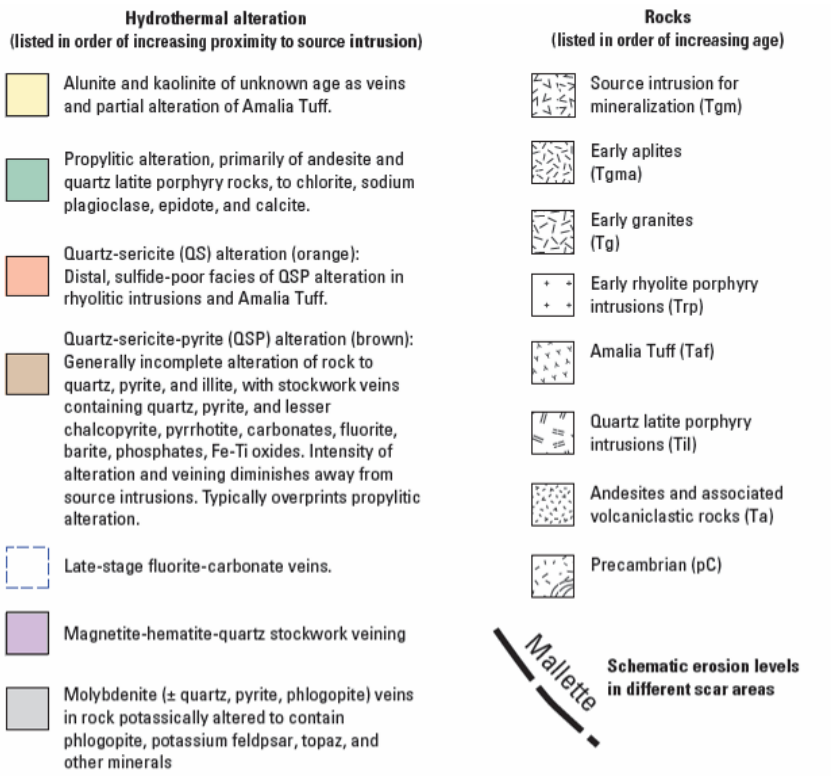

FIGURE 2. Cross section showing schematic spatial distributions of lithologies, alteration assemblages, and alteration scars in the Red River valley (taken from Ludington et al., 2005, which is modified from Martineau et al., 1977).

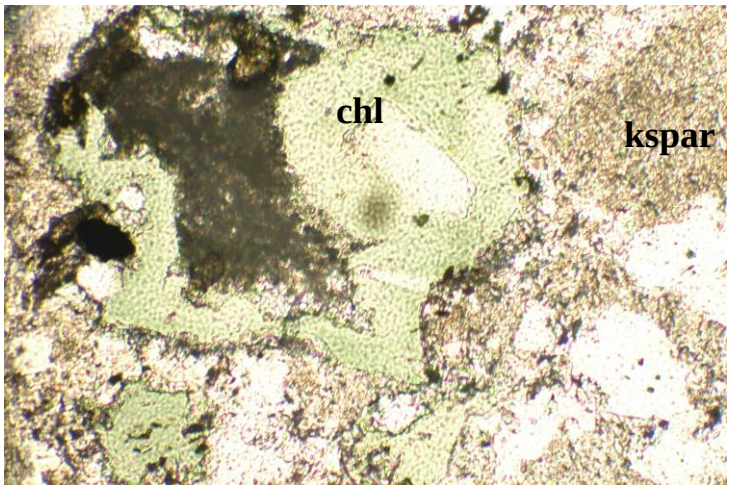

FIGURE 3. Propyllitic alteration as indicated by green chlorite (chl) and brown feldspar (kspar) minerals in sample GMG-PIT-0013 in plane polarized light; field of view is approximately 1.8 mm.

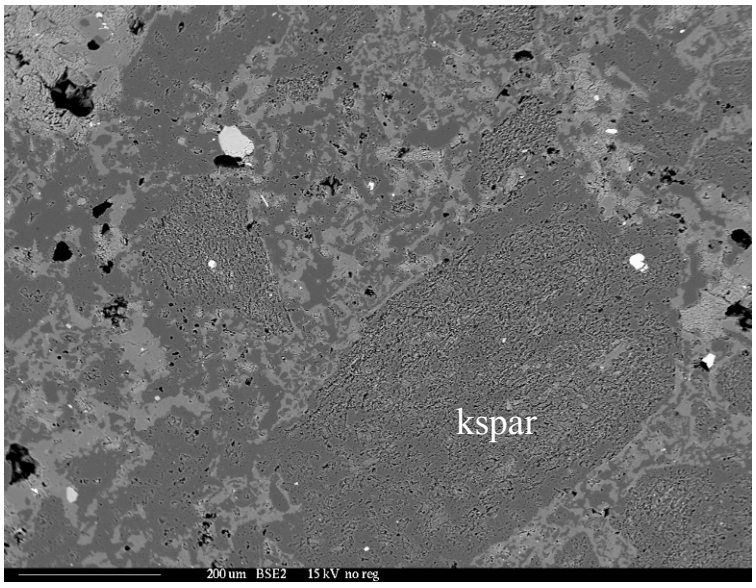

FIGURE 4. Backscattered electron microprobe image showing argillic alteration where clay minerals replacing feldspar phenocrysts (kspar) in sample PIT-KMD-0007.

Potassic alteration

Potassic alteration is typically the predominant type of hydrothermal alteration in the Questa area, but is not as predominant in the rock piles because it is directly associated with the molybdenum mineralization and these rocks went to the mill for processing. Potassic alteration at Questa, like most Climax-type deposits is characterized by the addition of potassium as secondary hydrothermal biotite, K-feldspar, and sericite along with quartz, fluorite, molybdenite, and pyrite as disseminations, veinlets and large crystals replacing the host rocks. Sericite includes the minerals illite, sericite, and/or muscovite. The major difference between these three K-micas is size: illite is a clay-size K-mica, whereas muscovite is larger. Sericite is of intermediate size. Some minor

compositional differences, especially in potassium content, also occur between the three minerals. Characteristic textures include large K-feldspar crystals and rimming of plagioclase by K-feldspar. Potassic alteration is one of the most pervasive alteration types in the Questa area and found in all rock types (Ludington et al., 2005). Stockwork magnetite-hematite veins with intergrown anhydrite/gypsum overlaps the potassic alteration along the edges of some veins (Martineau et al., 1977).

Phyllic or QSP alteration (Quartz-sericite-pyrite)

Phyllic or QSP (quartz-sericite-pyrite) alteration is widespread above the Questa molybdenum deposit, is typically above or overlaps the potassic alteration (Fig. 2), and is common within the rock piles and various lithologies in the Questa area. QSP alteration is defined by the predominance of quartz, sericite, and pyrite. QSP alteration typically is found as thin QSP veinlets cutting the host rock and as quartz, sericite, and pyrite replacing the groundmass and primary igneous minerals (Fig. 5, 6). The proportions of quartz, sericite, and pyrite vary according to the intensity of alteration. Typically quartz exceeds sericite, which exceeds pyrite in abundance. The amount of pyrite typically decreases away from the ore body. QSP alteration is commonly crosscut by intersecting stockwork veins, up to a few centimeters wide and consisting of quartz, pyrite, sericite, and rarely chalcopyrite, sphalerite, and galena.

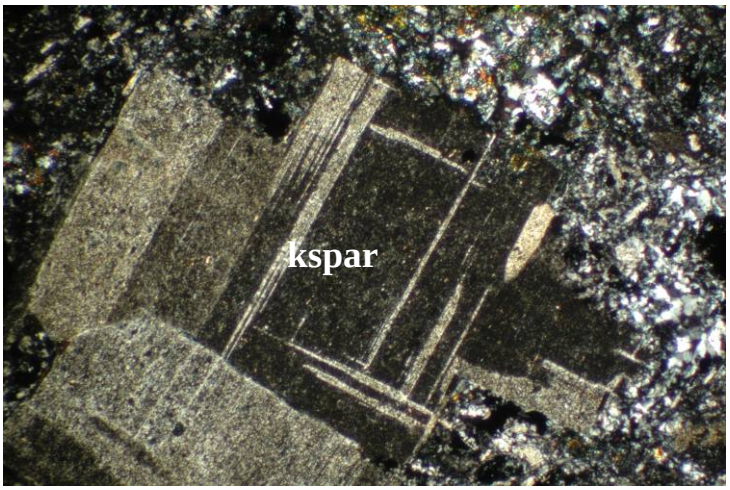

FIGURE 5. Sample PIT-LFG-0001 shows moderate QSP alteration under crossed polarized light; field of view is approximately 1.8 mm. The feldspar phenocryst (kspar) is well-defined and the groundmass is replaced by quartz and sericite.

Silicification

Silicification is produced by the addition of silica, predominantly as quartz. Quartz occurs as amygdule-fillings, fracture coatings, thin quartz veins, breccia cements, and as replacements of primary minerals. Silicification differs from the QSP alteration in that only replacement of quartz occurred without pyrite and sericite and is typically restricted to halos surrounding veins and within fault zones.

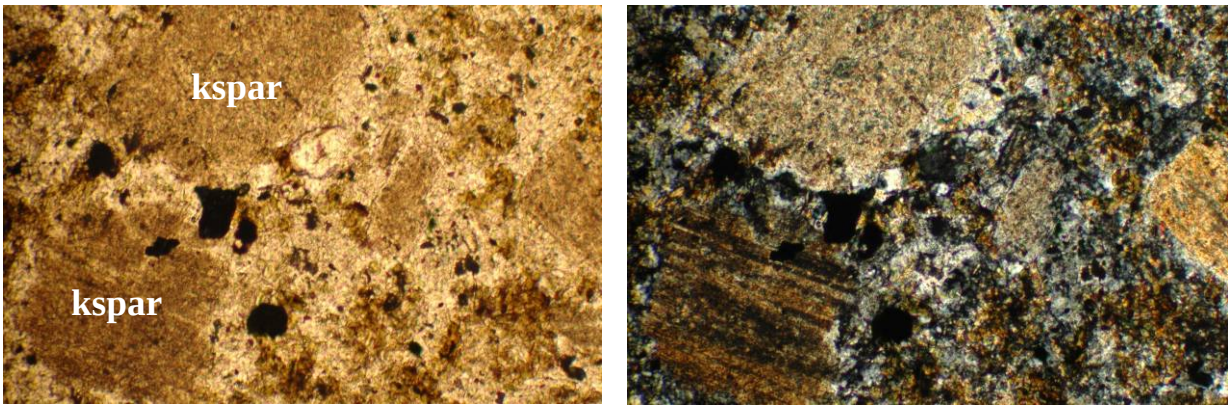

FIGURE 6. Sample PIT-KMD-0007 showing moderate to strong QSP alteration. The feldspar (kspar) phenocryst are replaced by quartz and sericite and the grain boundaries are poorly defined both in plain polarized light and under crossed polarized light; field of view is approximately 1.8 mm.

Carbonate-fluorite and magnetite-hematite veins

Intersecting veins of predominantly carbonate (manganiferous calcite, dolomite, rhodochrosite), anhydrite/gypsum, fluorite, and magnetite or hematite crosscut the molybdenum veins and potassic and QSP altered rocks near the ore body and within the alteration scars. Locally sericite/illite is found in some of these veins.

MINERALOGY

Petrographic and microprobe studies and review of the literature have identified the minerals in the Questa mine rock piles and probable elemental composition of these minerals, summarized in Table 3.

TABLE 3. Relative stabilities, approximate concentrations, and compositions of minerals found in Questa rock pile deposits (NM Tech electron microprobe results in bold, other elements by Molling, 1989; Shum, 1999; Piché and Jébrak, 2004; Plumlee et al., 2005). Tr=trace, Approx=approximate concentration in the Questa rock-pile materials

Relative stability	Mineral	Approx %	Primary elements	Trace elements	Formula
Easily weathered	pyrite	0-8	**Fe, S**	**Cu,** Te, Co, Pb	FeS_2
	calcite	0-5	**Ca, CO**	**Sr, Al, Mg, Mn, Fe, Si, Ba,** P	$CaCO_3$
	anhydrite	tr	Ca, S		$CaSO_4$
	hornblende	0-tr	Mg, Fe, Ca, Al, Si	Ni, Co, Mn, Sc, Si, V, Zn, Cu, Ga	
	Biotite/ phlogopite	0-13	K, Mg, Fe, Al, Si	F, Rb, Ba, Ni, Co, Li, Mn, V, Zn, Cu, Ga	$KFe_3AlSi_3O_{10}(OH)_2$
	apatite	0-1	**Ca, P, F**	**Si, S, Mn, Fe, Sr, Cl,** REE, Pb, Y	$Ca_5P_3O_{12}{\cdot}OH$
	jarosite	0-0.5	**Fe, S, H, K**		$KFe_3(SO_4)_2(OH)_6$
	alunite	0-0.5	S, K		
	copiapite	0-0.5	Fe, S		$Fe^{+2}(Fe^{+3})_4(SO_4)_6(OH)_2{\cdot}20H_2O$
	sphalerite	0-0.1	**Zn, S**	Cd	ZnS
	chalcopyrite	0-0.1	**Cu, Fe, S**		$CuFeS_2$

Relative stability	Mineral	Approx %	Primary elements	Trace elements	Formula
	melanterite	0-0.1	Fe, S		$Fe(SO_4)\cdot 7H_2O$
	schwertmannite	0-0.1	Fe, S		$Fe_8O_8(OH)_6SO_4\cdot nH_2O$
	galena	0-0.1	Pb, S	Ag	PbS
Moderately weathered	fluorite	0-0.1	Ca, F	Y	CaF_2
	dolomite	0-0.1	**Mg, Ca, CO**	**Sr, Al, Mg, Mn, Fe, Si, Ba**	$MgCa(CO_3)_2$
	rhodochrosite	0-0.1	**Mn, Ca, CO**		$MnCO_3$
	albite		**N, Al, Si**	Cu, Ga, **Ba, Sr,**	$NaAlSi_3O_8$
	orthoclase	0-24	**K, Al, Si**	Rb, **Ba, Sr,** Cu, Ga	$KAlSi_3O_8$
	anorthite	0-20	**Ca, Al, Si**	**Ba, Sr,**	$CaAl_2Si_2O_8$
	Muscovite (sericite, illite)	0-30	**K, Al, Si**	**F, Cl, Ti, Cr, Mg, Na, Ca, Mn, Fe**, Rb, Ba, Sr, Ga, V, Be?, Li?	$KAl_2(Si_3Al)O10(OH)_2$
	magnetite	0-1	**Fe, Ti**	**Al, Mg, Ca, Mn,** Zn, Co, Ni, **Cr**, V	Fe_3O_4
	Epidote	0-16	**Ca, Al, Si**	**Cr, Mg, Mn, Fe, Na, Ti**	$CaFeAl_3(SiO_4)_3(OH)$
	chlorite	0-12	Fe, Al, Mg, Si, Be?	F, Be?, Li?, various	$Mg_3Fe_2Al_2Si_3O_{10}(OH)_8$
	smectite	0-24	**Si, Al, Mg, Ca, Na, K,** Be?	**P, S, Ti, Mn, Fe, F, Cl,** Be?, Li?	$Ca0_{.33}(Mg0_{.66}Al_{3.34})(Si_8)(OH)_4$
	chromite	0-0.1	Fe, Cr		$FeCrO_4$
	titanite	0-0.1	Ca, Ti, Si		$CaTiSiO_4\cdot OH$
	rutile	0-0.1	Ti		TiO_2
	beryl	0-0.01	Be		BeO
	barite	0-0.01	Ba, S	Sr	$BaSO_4$
	actinolite	0-1	Ca, Mg, Si, OH		$Ca_2Mg_5Si8O_{22}(OH)_2$
Very stable	quartz	0-66	Si		SiO_2
	kaolinite	0-7	**Al, H, Si**	F, Cl	$Al_2Si_2O5(OH)_4$
	gypsum	0-20	**Ca, S**	**Sr, Ba**	$CaSO_3\cdot H_2O$
	ferrihydrite	0-0.01	**Fe**		$Fe(OH)_3$
	hematite	0-10	**Fe**	Various	
	goethite	0-1	Fe	Various	FeOOH
	FeMnTi oxides	0-10	Fe, Mn, Ti	various	
	molybdenite	0-0.1	Mo, S		MoS
	Amorphous Si, Fe, Mn, Al	?	Si, Fe, Mn, Al	various	various

Clay mineralogy

Several outcrop and drill core samples were examined for their clay mineralogy by using X-ray diffraction (XRD) techniques to identify the clay minerals present in the Questa rock materials (Fig. 7). Different lithologies and hydrothermal-alteration assemblages were chosen. The host-rock lithology is one of the main factors controlling the clay mineral assemblages due to the presence or absence of certain primary minerals, such as amphiboles and micas. For example, high abundances of chlorite are found almost exclusively in andesitic rock types (Fig 7a). However, the results of the XRD analyses indicate another controlling factor in the clay mineral assemblage is the type of hydrothermal alteration. The QSP-altered samples of andesite and rhyolite composition result in similar mineral assemblages of predominantly illite and minor kaolinite (Fig. 7b). Over-printing of alteration mineral assemblages results in samples containing each of the clay-mineral groups (illite, kaolinite, chlorite, smectites, mixed layered clays) despite

a difference in host rock lithology (Fig. 7c). The drill-core samples collected near the center of the ore deposit have more than one type of over-printing hydrothermal alteration mineral assemblage due to the nature of the ore deposit.

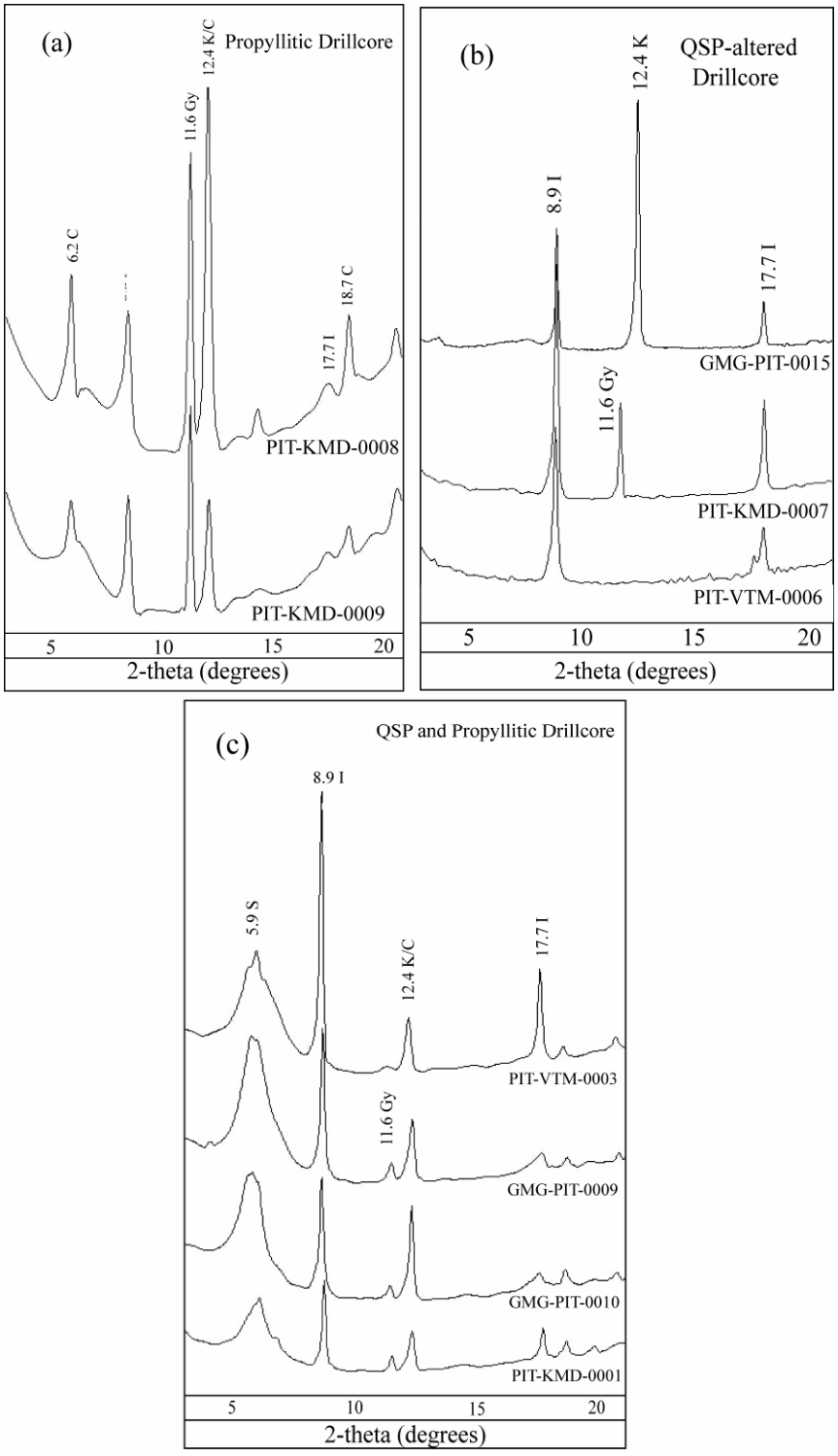

FIGURE 7. a) The XRD results of drill-core clay analyses of propllytically altered andesite samples, b) the XRD results of andesite and rhyolite QSP-altered core samples

and c) andesite and rhyolite drill core samples with evidence of over-printing hydrothermal alteration assemblages. I = illite, K = kaolinite, C = chlorite, S = smectite, Gy = gypsum.

LITHOLOGIC DESCRIPTIONS

Felsic Intrusions

Goathill Porphyry

The Goathill Porphyry (Table 4) is a major intrusion that forms Goat Hill, west of the rock piles and the pit (Figs. 8, 9). Numerous dikes of the Goathill Porphyry cut the overburden and the open-pit deposit. This porphyry was intruded after or during the molybdenite mineralization. It is characterized by an aphanitic groundmass with 15-20% phenocrysts that consist of quartz (large crystals >5mm), plagioclase, orthoclase, and minor mafic minerals, but hornblende is absent. The large quartz phenocrysts are typically round or oval; whereas the feldspars are large blocky, cream-colored phenocrysts. A rare rapakivi texture can be present where the K-feldspars are rimmed with plagioclase. Some company and other descriptions refer to a quartz-feldspar porphyry that is now considered to be equivalent to the Goathill Porphyry.

FIGURE 8. Sample ROC-VTM-G005 showing typical propylitic texture of the cream-colored Goathill Porphyry.

FIGURE 9. Sample ROC-VTM-G011 is QSP-altered Goathill Porphyry. Note the holes caused by loss of quartz phenocrysts. This rock in a weathered state would be stained yellow.

TABLE 4. Summary descriptions of felsic intrusions. Sample locations are given in the UTM column (zone 13). na indicates the UTM coordinates are not available for the sample (samples are from the Chevron rock collection).

Symbol	color	Mineralogy (weight %)	Structure/texture	Photograph number	UTM Easting, Northing (meters)
Tghp (Goathill Porphyry)	Cream colored groundmass	Quartz, plagioclase, orthoclase, minor mafics	Porphyritic texture	ROC-VTM-G005	na
Altered Tghp	white	Quartz, pyrite	Porphyritic texture with holes (loss of quartz phenol)	ROC-VTM-G011	na
Thfp Christmas Tree porphyry	Cream colored groundmass	Quartz, plagioclase, orthoclase, hornblende	Porphyritic texture	ROC-VTM-G007, ROC-VTM-G008, PIT-KMD-0001	na na 454185.6, 4062159
Altered Thfp Christmas Tree porphyry	Light gray	Quartz, plagioclase, orthoclase, hornblende, pyrite	Fine grained porphyritic texture, QSP alteration	ROC-VTM-G026	na
Tpap, Tap Aplite		quartz, orthoclase, plagioclase, biotite, hornblende	Porphyritic texture, less phenocrysts than Tghp, Thfp	ROC-VTM-G010	na
QSP altered Tpap	White with yellow staining	Quartz, feldspar casts, trace pyrite	Fine grained porphyritic texture	ROC-VTM-G027 ROC-MZQ-0006 ROC-MZQ-0021	na 455737, 4060977 454281, 4042533
Tgp	Pink to cream	Quartz, biotite, hornblende, feldspar, pyrite	Porphyritic texture	ROC-VTM-G012 PIT-VCV-0016	na

Christmas Tree porphyry or Hornblende feldspar porphyry

The hornblende feldspar porphyry (Table 4) is the major porphyritic intrusion in the open-pit area, especially along strike of the NE zone and is locally referred to as the Christmas Tree porphyry (Fig. 10-15). It has a cream-colored aphanitic groundmass that is a phenocryst-rich porphyry with abundant broken crystals of black, tabular to blocky to square hornblende; clear, round to oval quartz; and large, cream, blocky feldspar phenocrysts. Characteristically the phenocrysts consist of 6-10% (2-5 mm) anhedral (often vermicular) quartz, 20-25% (2-20 mm) subhedral orthoclase, 6-8% (3-8 mm) subhedral plagioclase, 4-6% (1-4 mm) subhedral biotite, 2-5% (2-8 mm) euhedral hornblende, and as much as 1-3% magnetite. There are two compositions depending upon the quartz concentration: rhyolite and quartz latite. Pyrite (3-5%) is common as disseminations, thin fracture-fillings, and along phenocrysts boundaries. Rimmed feldspars are locally common. The Christmas Tree porphyry can include large blocks of andesite and rhyolite (Amalia Tuff) as a megabreccia.

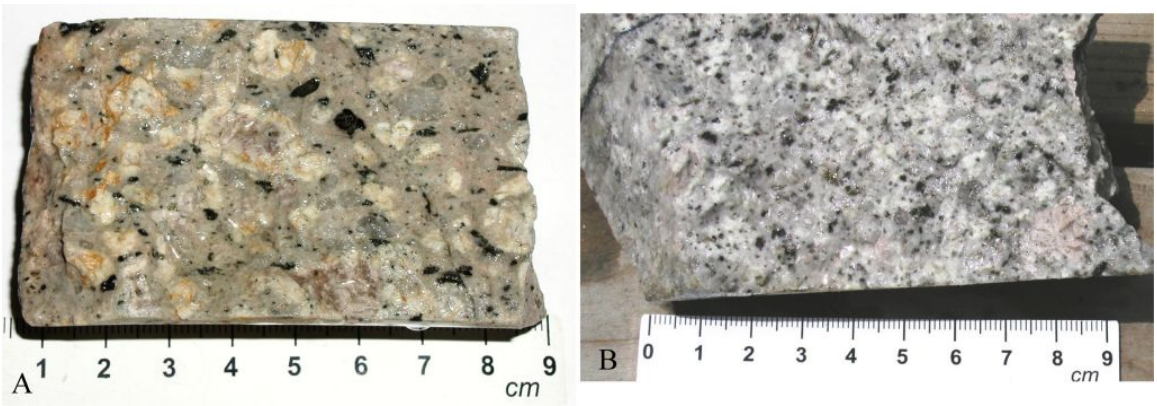

FIGURE 10. (A) Sample ROC-VTM-G007 is coarse-grained, cream-colored, phenocryst-rich Christmas Tree Porphyry (Thfp) with black hornblende, clear quartz, and cream feldspar phenocrysts. (B) Sample PIT-KMD-0001 showing hand sample of cream-colored, porphyritic, Christmas Tree Porphyry.

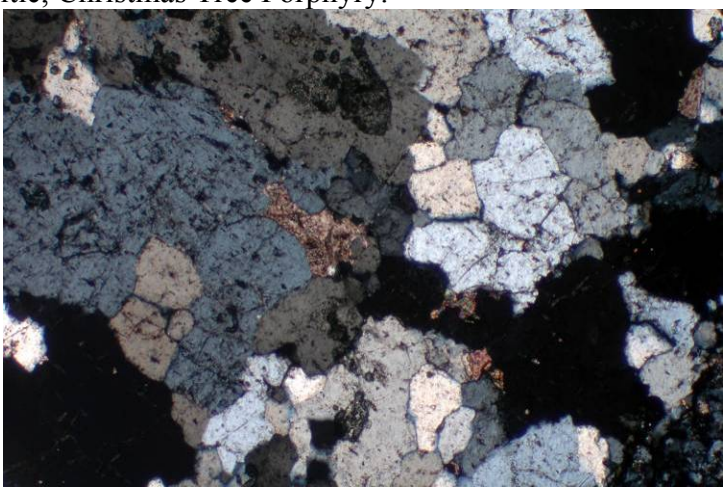

FIGURE 11. Thin section of sample PIT-KMD-0001 showing Christmas Tree porphyry, consisting of quartz, feldspar, calcite, clays and trace amounts of pyrite, magnetite and biotite. Magnification is 5 times and field of view is 1.8 mm.

FIGURE 12. Sample ROC-VTM-G008 is coarse-grained, cream-colored, phenocryst-rich Christmas Tree porphyry intruded by a small cream-colored aplite dike.

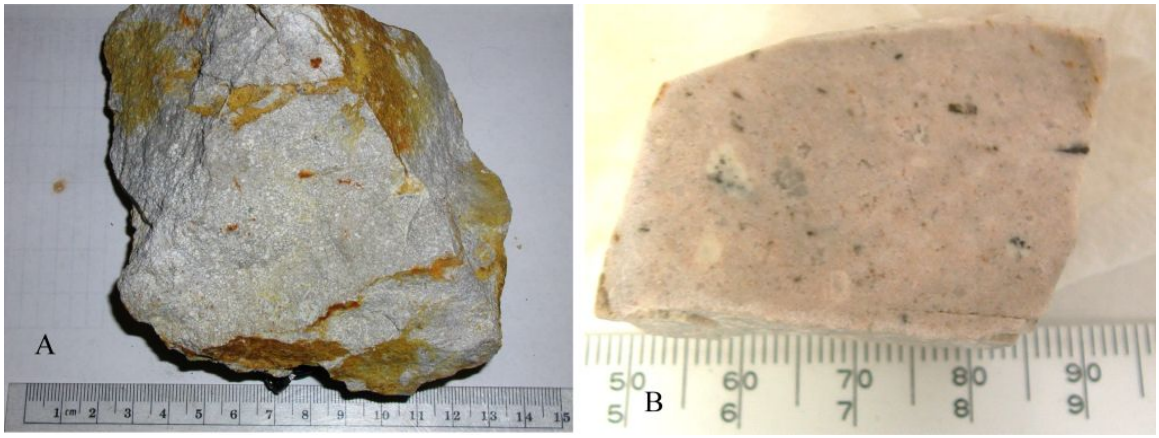

FIGURE 13. (A) Sample ROC-VTM-G027 is QSP-altered aplite porphyry with trace of pyrite. (B) Sample PIT-VCV-0028 is QSP-altered aplite porphyry with fresh disseminated pyrite.

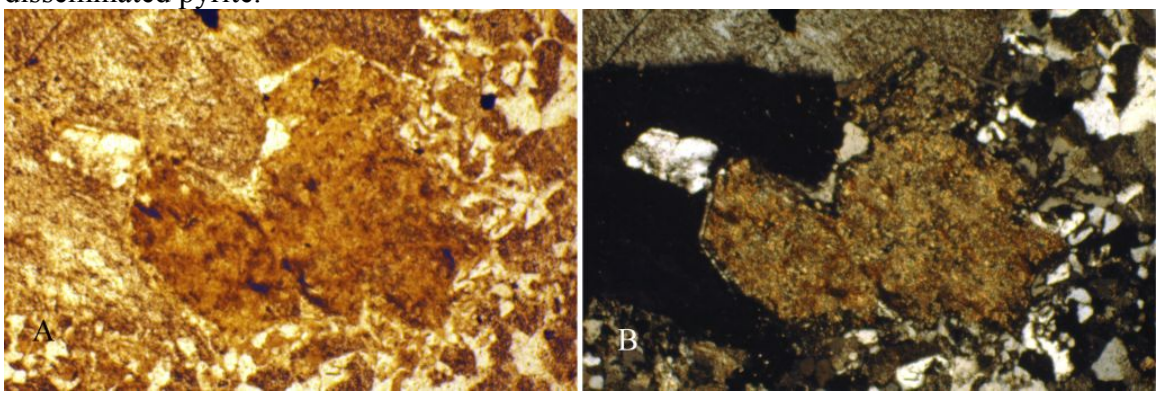

FIGURE 14. Thin section photographs of sample PIT-VCV-0028 showing QSP-altered aplite, under plane polarized light (A) and with crossed polarized light (B), 5 times magnification and a field of view of approximately 1.8 mm. Illite has replaced the feldspar phenocryst.

FIGURE 15. Sample ROC-VTM-G026 is fine-grained (aplitic) phase of the QSP-altered Christmas Tree porphyry consisting of very small quartz, feldspar, and hornblende phenocrysts and 5% disseminated pyrite.

Plagioclase (biotite) aplite porphyry

The primary granitic porphyry in the open pit is the plagioclase aplite porphyry (Table 4), which is an allotriomorphic, granular aplitic groundmass of quartz, orthoclase, plagioclase and minor mafic minerals with 0-2% (2-5 mm) anhedral quartz, 3-6% (2-7 mm) subhedral orthoclase, 4-8% (2-10 mm) subhedral biotite, and trace hornblende (Figs. 16-17). It appears to grade into finer-grained allotriomorphic granites at depth, with a fine-grained aplitic matrix containing abundant minute (0.25-1 mm) crystals of quartz and orthoclase with 2-6% (2-6 mm) anhedral quartz, 2-5% (1-3 mm) subhedral orthoclase, 4-8% (2-6 mm) subhedral plagioclase, 3-6% (0.5-4 mm) euhedral hornblende. The Near Aplite (fine sub-aplitic matrix of quartz, orthoclase, plagioclase, and abundant fine biotite) occurs along contact of aplite just beneath other volcanic rocks and is interpreted to represent a hybrid derived by assimilation of andesite as aplite intrusions intruded into the volcanic pile.

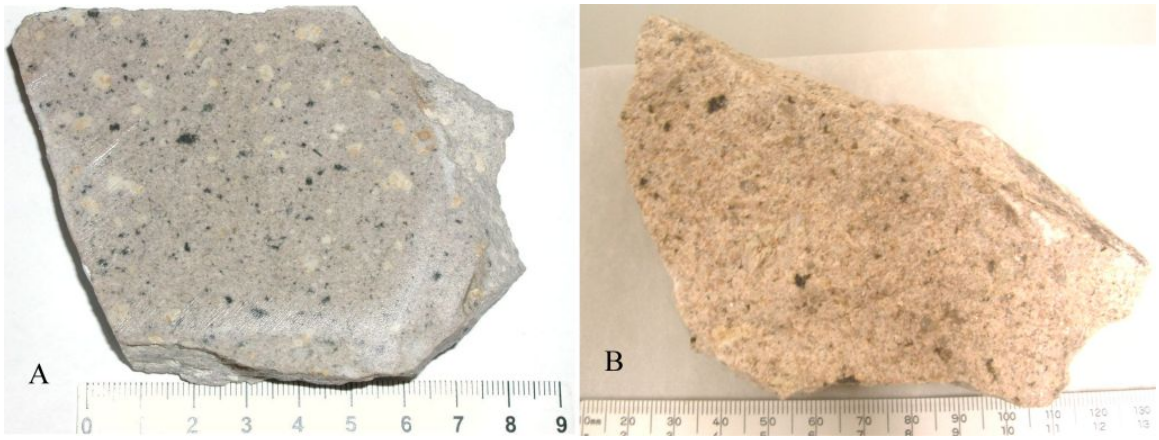

FIGURE 16. (A) Sample ROC-VTM-G010 is pink, plagioclase aplite porphyry to porphyritic aplite with quartz, feldspar, and biotite phenocrysts. (B) Sample ROC-MZQ-0006 is peach-colored, fine-grained, plagioclase aplite.

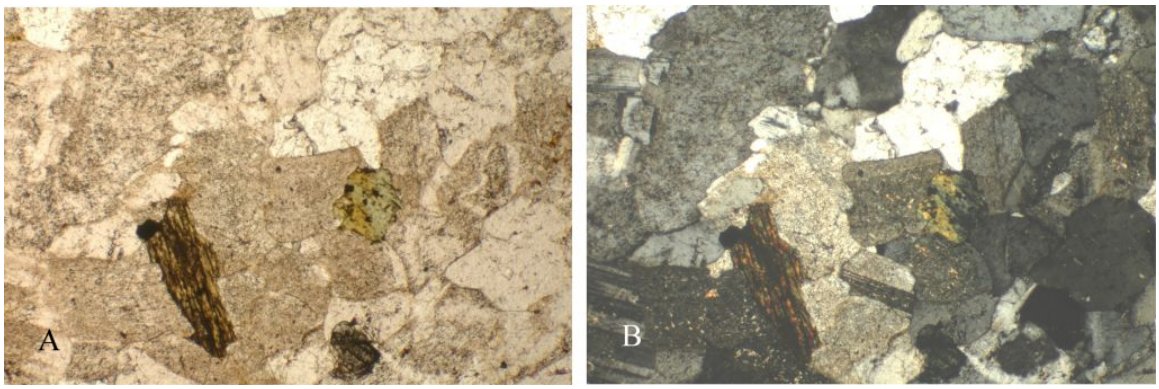

FIGURE 17. Thin section photograph of sample ROC-MZQ-0006 showing aplite with quartz, feldspar and some biotite under normal polarized light (A) and crossed polarized light (B). Magnification is 5 times and field of view is 1.8 mm.

Granite porphyry

The granite porphyry is a porphyritic intrusion with a phaneritic matrix, coarse allotriomorphic to hypidiomorphic textures, and consists of 30% (0.5-2 mm) quartz, 35% (0.5-3 mm) orthoclase, 20% (0.5-3 mm) plagioclase, 1% (0.25-2 mm) subhedral biotite (Figs. 18-19). The phenocrysts include 8-10% (3-10 mm) anhedral to subhedral quartz and 4-6% (3-12 mm) subhedral orthoclase.

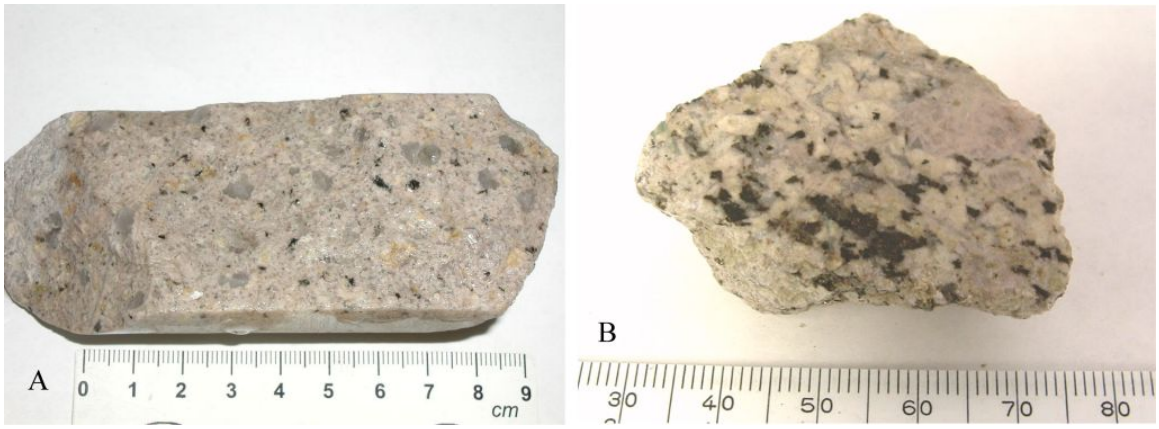

FIGURE 18. (A) Sample ROC-VTM-G012 is granite porphyry from the underground deposit. (B) Sample PIT-VCV-0016 is granite porphyry with pink feldspars, quartz, and greenish-black micas.

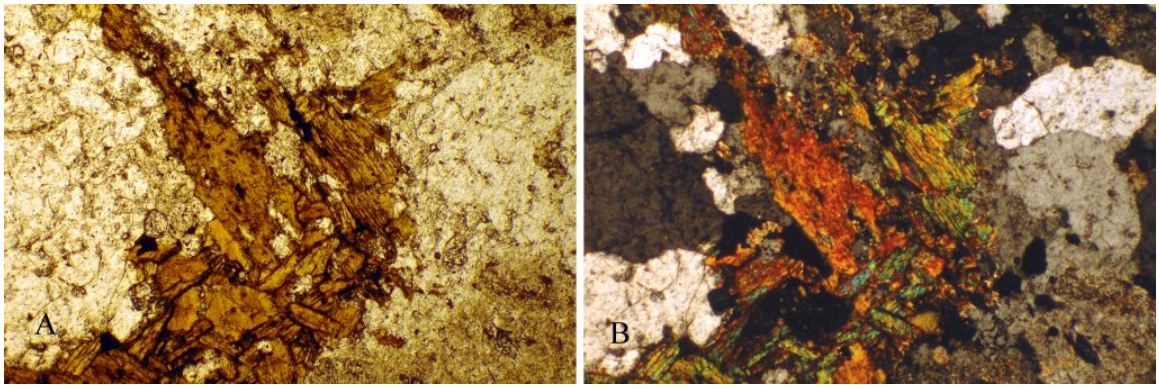

FIGURE 19. Thin section photos of sample PIT-VCV-0016 under normal polarized light (A) and crossed polarized light (B) with quartz, feldspars, and micas, 5 times magnification and field of view of approximately 1.8 mm.

Amalia Tuff

The Amalia Tuff is a welded, gray to reddish brown rhyolite ignimbrite (ash flow tuff) that typically contains 10-20% phenocrysts of alkali feldspar (albite-orthoclase) and quartz with sparse ferrohedenbergite, fayolite, and sodic amphibole (Figs. 20-32). The eutaxitic texture or flow banding produce by flatten pumice fragments is characteristic of the Amalia Tuff. Pumice is common in fresh samples and typically characterizes the foliation or flow banding. Quartz typically is found as round to oval phenocrysts that are typically persistent even in highly altered and weathered rock. Some confusion has existed in the literature and company descriptions as to the extent and correlations of the Amalia Tuff. It is now believed that what was called the Pit Porphyry and Capulin Quartz

Porphyry are not intrusions, but ash flow tuffs belonging to the Amalia Tuff. At the base of the Amalia Tuff, fragmental tuff and mudflow units are found locally. These units are a component within the open-pit deposit and overburden and are found in the rock piles. Sample descriptions for the QRPWASP should include the appropriate symbols as listed in Table 5.

TABLE 5. Summary descriptions of Amalia Tuff. na indicates the UTM coordinates are not available for the sample.

Symbol	color	Mineralogy (weight %)	Structure/texture	Photograph number	UTM Easting, Northing (meters)
Topt	gray	Quartz phenocrysts, feldspar	welded, black obsidian pumice forming flow banding	ROC-VTM-G001, ROC-VTM-G002	na na
QSP Trt	Gray to brown	Quartz phenocrysts, pyrite	flow banding, QSP	ROC-VTM-G030 ROC-MZQ-0004	na 462734, 4065869
Tpp	gray	Quartz phenocrysts, feldspar	welded, flow banding (no obsidian remaining)	ROC-VTM-G003, ROC-VTM-G019	na na
Tdqpt	Reddish brown to gray	Quartz phenocrysts, feldspar	Welded, flow banding, white stretched pumiceous fragments	ROC-VTM-G004	na
Trt	Gray and black	Andesite fragments	Mudflow at base of Amalia Tuff	ROC-VTM-G009	na
Tcqp Capulin quartz porphyry			Rhyolite with eutaxitic texture		
Tcrt Crystal rich tuff	Gray	Feldspar, quartz, rock fragments, pumice fragments	Flow banding	ROC-VTM-G020	na

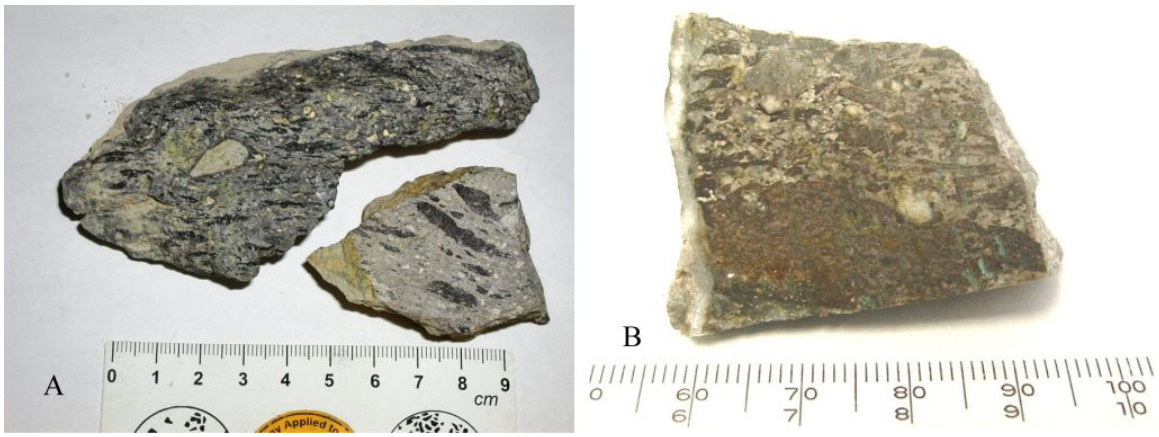

FIGURE 20. (A) Sample ROC-VTM-G001 is welded Amalia Tuff showing flow banding formed by black obsidian (pumice) foliation. (B) Sample PIT-VCV-0002 is hand sample of Amalia Tuff with flow banding and remnant obsidian and pumice fragments.

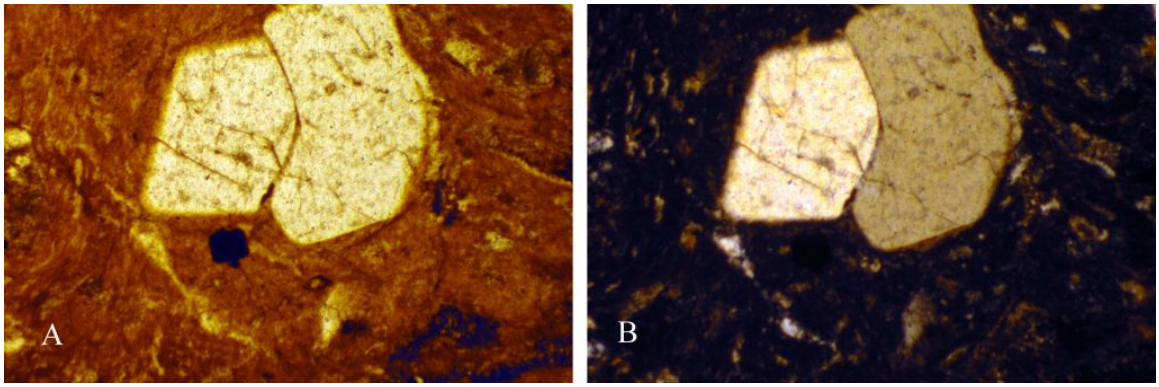

FIGURE 21. Thin section photographs of sample PIT-VCV-0002 under normal plane polarized light (A) and crossed polarized light (B) showing flow banding around quartz phenocrysts, 5 times magnification and field of view of approximately 1.8 mm.

FIGURE 22. (A) Sample ROC-VTM-G002 is welded Amalia Tuff showing flow banding formed by black obsidian (pumice) foliation (Topt). (B) Sample PIT-VTM-0006 is slightly QSP-altered drill core of Amalia Tuff with flow banding.

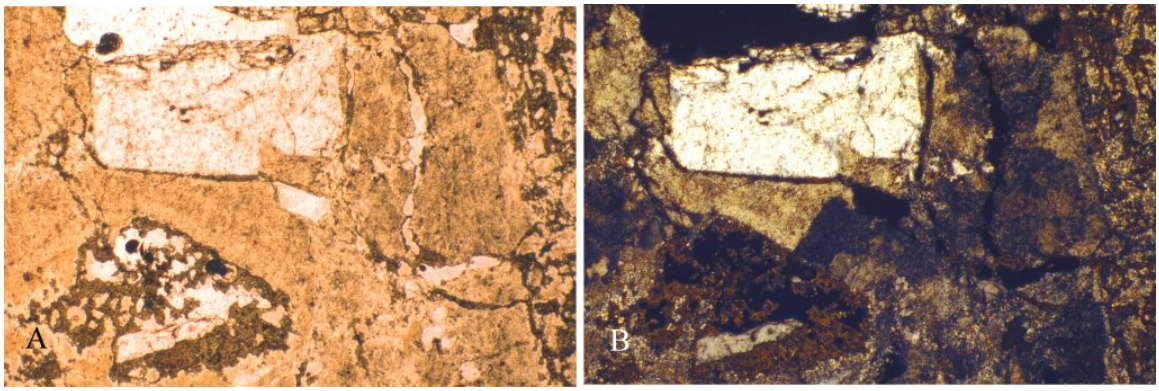

FIGURE 23. Thin section photographs of sample PIT-VTM-0006 under normal plane polarized light (A) and crossed polarized light (B) showing flow banding surrounding feldspar phenocrysts, 5 times magnification and field of view of approximately 1.8 mm.

FIGURE 24. Sample ROC-VTM-G003 is flow-banded rhyolite tuff (Amalia Tuff) showing eutaxitic foliation. Misnamed as pit porphyry.

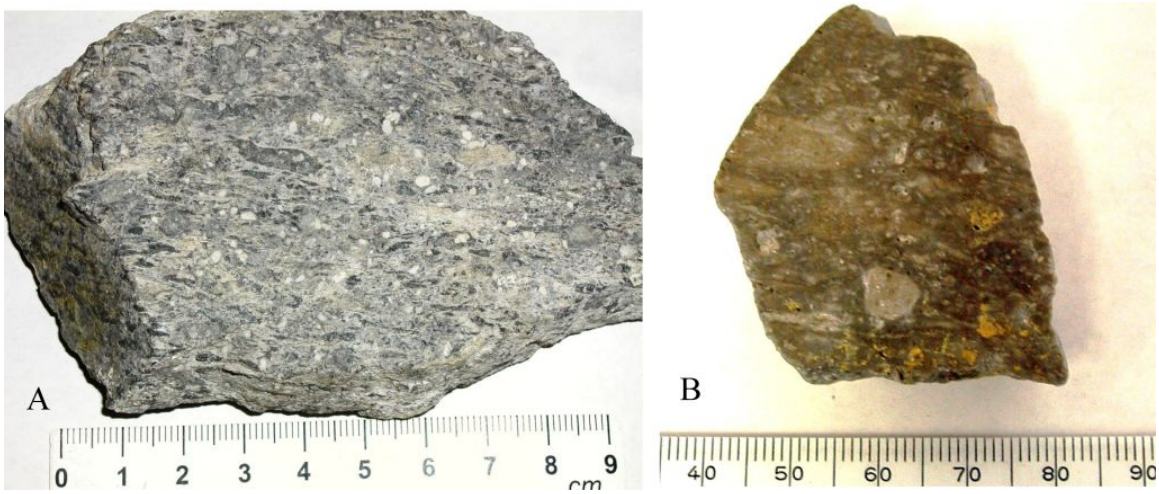

FIGURE 25. (A) Sample ROC-VTM-G019 is slightly porphyritic rhyolite with foliation. Small pyrite cubes disseminated in rock. Called pit porphyry, but is actually Amalia Tuff. (B) Sample PIT-VCV-0006 is hand sample showing porphyritic texture and remnant flow banding.

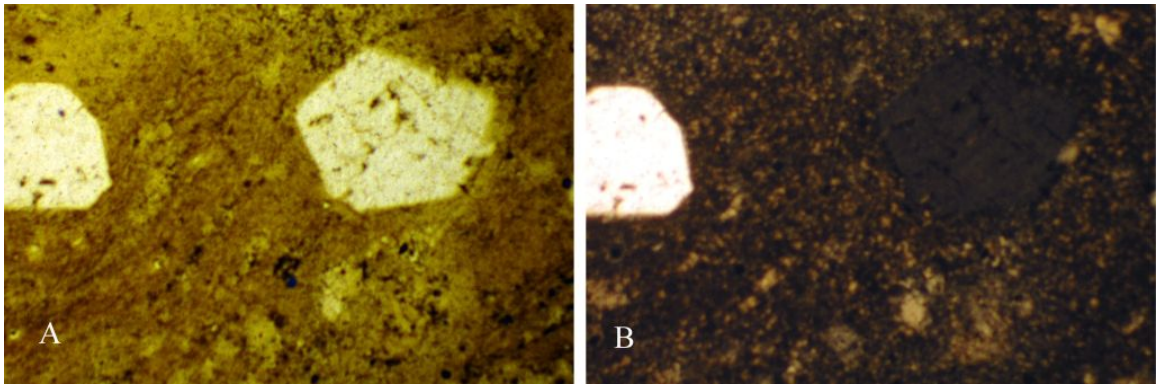

FIGURE 26. Thin section photographs of sample PIT-VCV-0006 under normal plane polarized light (A) and crossed polarized light (B) showing flow banding around quartz

and feldspar phenocrysts, 5 times magnification and field of view of approximately 1.8 mm.

FIGURE 27. Sample ROC-VTM-G004 is flow-banded rhyolite tuff, Amalia Tuff, typical of outflow units.

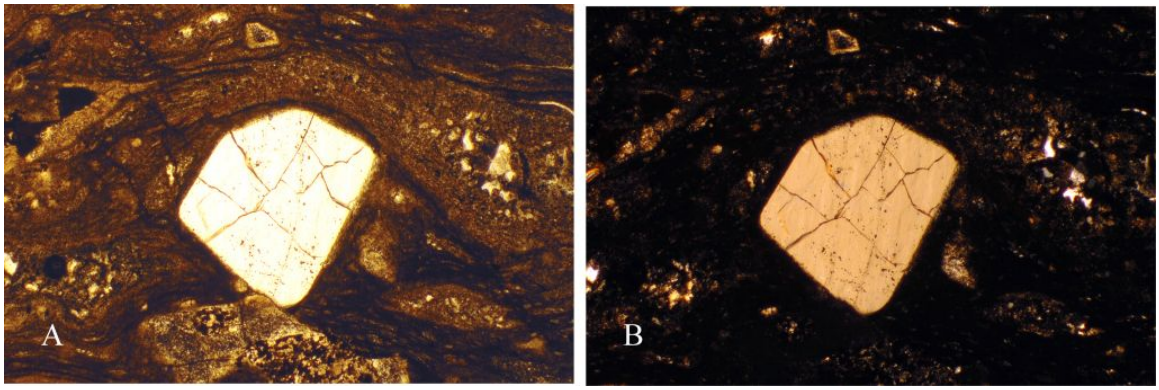

FIGURE 28. Thin section photographs of sample PIT-LFG-0011 under normal plane polarized light (A) and crossed polarized light (B) showing flow banding around quartz phenocrysts, 5 times magnification and field of view of approximately 1.8 mm.

FIGURE 29. Sample ROC-VTM-G030 is QSP-altered Amalia Tuff with remnant flow banding and 1% pyrite.

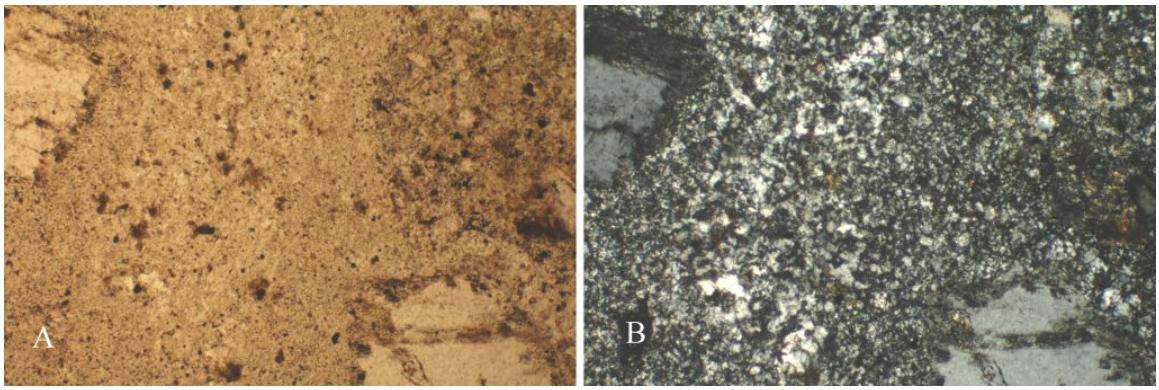

FIGURE 30. Thin section photographs of sample ROC-MZQ-0004, Amalia Tuff, under normal plane polarized light (A) and crossed polarized light (B) showing quartz and sanidine. Magnification is 5 times and field of view is 1.8 mm.

FIGURE 31. Sample ROC-VTM-G020 showing two phases of Amalia Tuff, pumice flow banding and crystal rich. Note crystals are broken.

FIGURE 32. Sample ROC-VTM-G009 is mudflow facies of the Amalia Tuff (Trt), typically found at the rhyolite flow, with an andesite fragment.

Latir Volcanic Rocks

The Latir volcanic rocks consist primarily of andesite, latite, dacite, and quartz latite lava flows with interbedded mudflows, sandstones, and breccias (Table 6).

Coarse-grained porphyritic andesite

The coarse-grained porphyritic andesite contains as much as 30% (5 mm) euhedral plagioclase, 1-8% (1-5 mm) euhedral biotite, 1-10% (2-8 mm) euhedral hornblende, and 0-5% (1-3 mm) subhedral quartz (Figs. 33-36). It is found as extensive flows up to 200 ft thick.

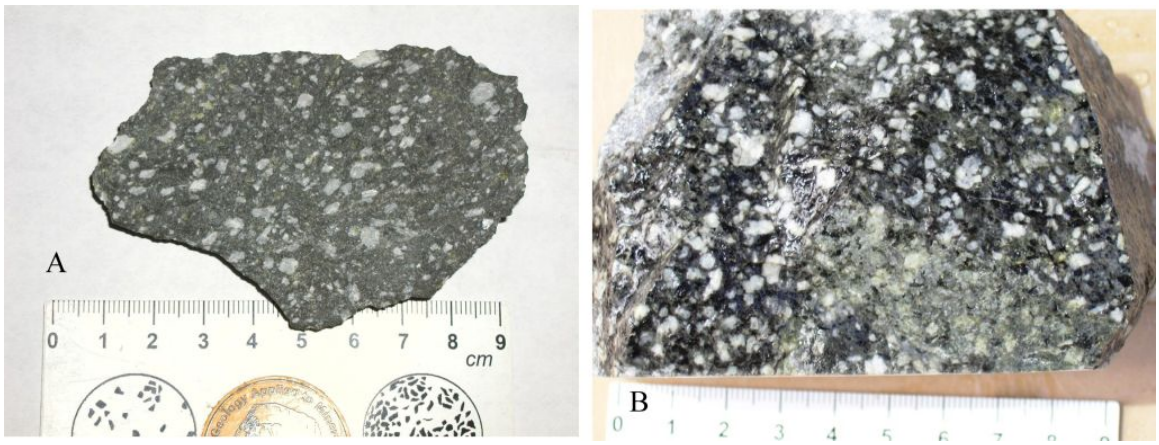

FIGURE 33. (A) Sample ROC-VTM-G015 is relatively fresh andesite of the Latir volcanics sequence. (B) Sample PIT-KMD-0009 is porphyritic andesite with some propylitic alteration.

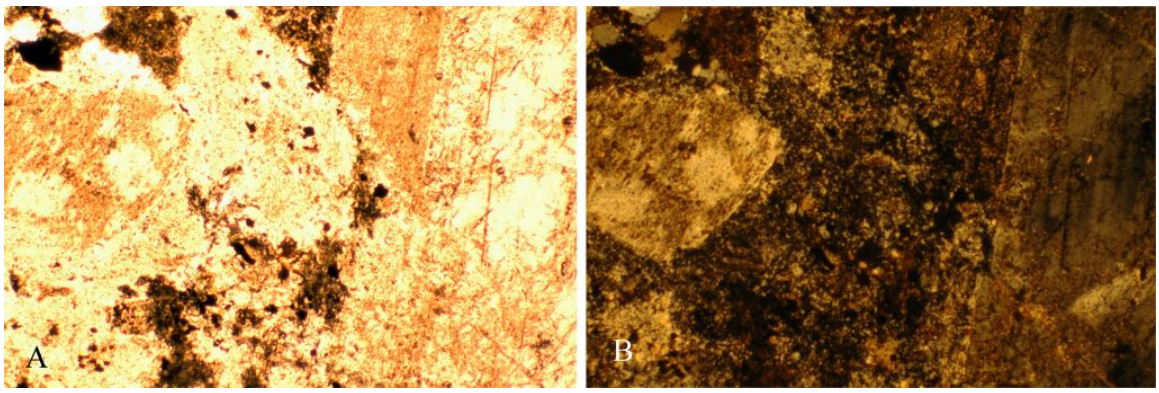

FIGURE 34. Thin section photographs of sample PIT-KMD-0009, andesite under normal plane polarized light (A) and crossed polarized light (B) showing propylitically-altered feldspars (cream colored) and chlorite (green) minerals. Feldspars show replacement by illite (brown). Magnification is 5 times and field of view is approximately 1.8 mm.

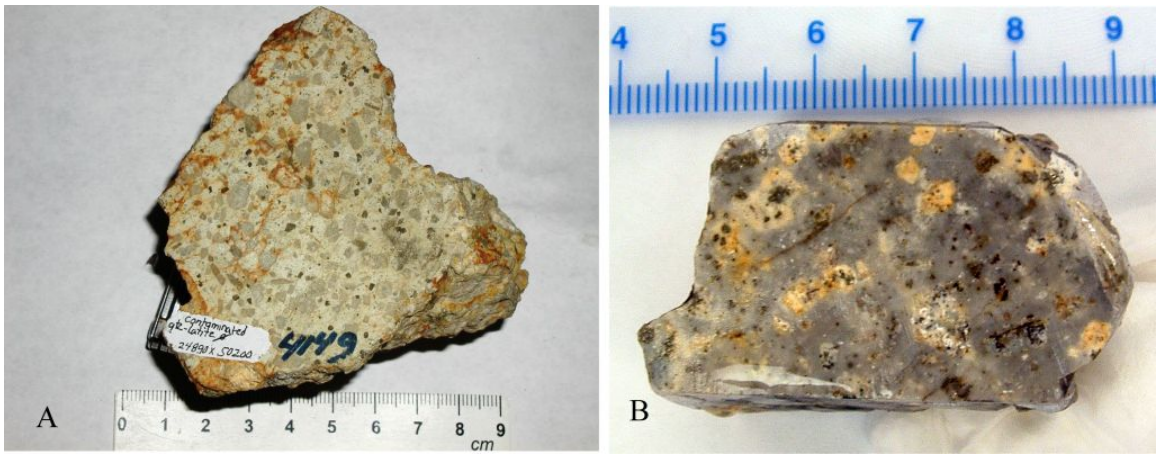

FIGURE 35. (A) Sample ROC-VTM-G017 is yellow and reddish stained quartz latite of the Latir volcanics with phenocrysts. (B) Sample GMG-PIT-0015 is hydrothermally-altered porphyritic andesite sample.

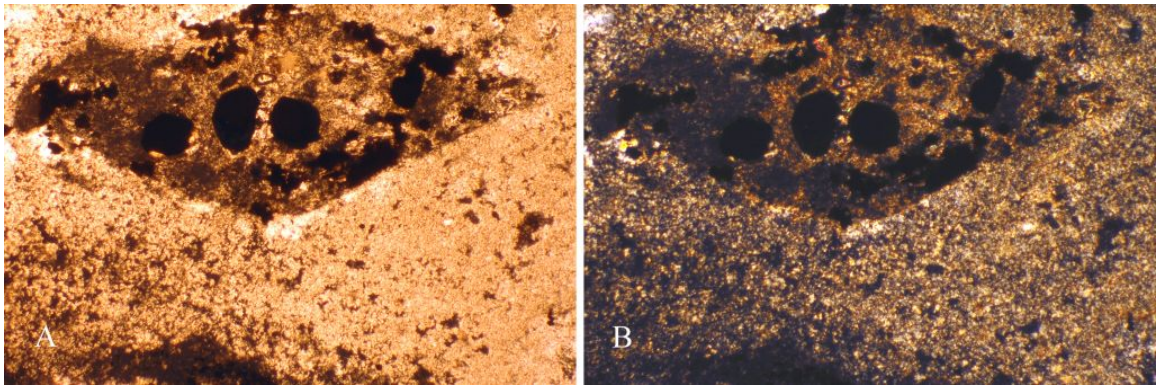

FIGURE 36. Thin section photographs of sample GMG-PIT-0015, andesite under normal plane polarized light (A) and crossed polarized light (B) showing a highly altered relic hornblende crystal with pyrite inclusions in a fine-grained groundmass, 5 times magnification and field of view of approximately 1.8 mm.

TABLE 6. Summary descriptions of Latir volcanic lithologies. No locations of samples are available.

Symbol	color	Mineralogy	Structure/texture	Photograph number
Tancp	Dark gray	Quartz and feldspar phenocrysts	Weak foliation, porphyritic	ROC-VTM-G015 PIT-KMD-0009
Altered Tancp	White to light gray	Quartz and feldspar phenocrysts, stained by Fe oxides	porphyritic	ROC-VTM-G017
Tan	Light gray	Phenocrysts of feldspar, biotite, and hornblende in fine-grained matrix.	porphyritic	ROC-VTM-G016
Tan	Greenish gray	Propylitic alteration (chlorite, epidote, pyrite)	porphyritic	ROC-VTM-G021 PIT-VCV-0010
Tanbx	Greenish gray to purplish gray	Prophylitic alteration (chlorite, pyrite)	breccia	ROC-VTM-G024 MIN-VTM-0001
Tan, Tana	Gray	QSP altered andesite	Porphyritic, fine	ROC-VTM-G025

Symbol	color	Mineralogy	Structure/texture	Photograph number
			grained	PIT-KMD-0007
Tql	Gray	Feldspar and hornblende phenocrysts	porphyritic	ROC-VTM-G013
Tanfp Finely porphyritic andesite	Greenish gray	Small feldspar phenocrysts	Porphyritic, matrix supported, phyllic alteration	ROC-VTM-G022, ROC-VTM-G031
Tbr biotized andesite	black	Biotite altered andesite	Fine grained	ROC-VTM-G014
Tanbx, Twb Andesite breccia	Black to gray to green	Andesite breccia fragments in fine grained matrix	Breccia, also known as water melon breccia	ROC-VTM-G028, ROC-VTM-G029

Fine-grained porphyritic andesite

The fine-grained porphyritic andesite contains as much as 30% (5 mm) euhedral plagioclase, 1-8% (1-5 mm) euhedral biotite, 1-10% (2-8 mm) euhedral hornblende, and 0-5% (1-3 mm) subhedral quartz (Figs. 37-42). It is found as extensive flows up to 200 ft thick and as minor dikes and sills.

FIGURE 37. Sample ROC-VTM-G016 is light gray porphyritic, crystal-rich andesite of the Latir volcanics with feldspar, biotite, and hornblende phenocrysts.

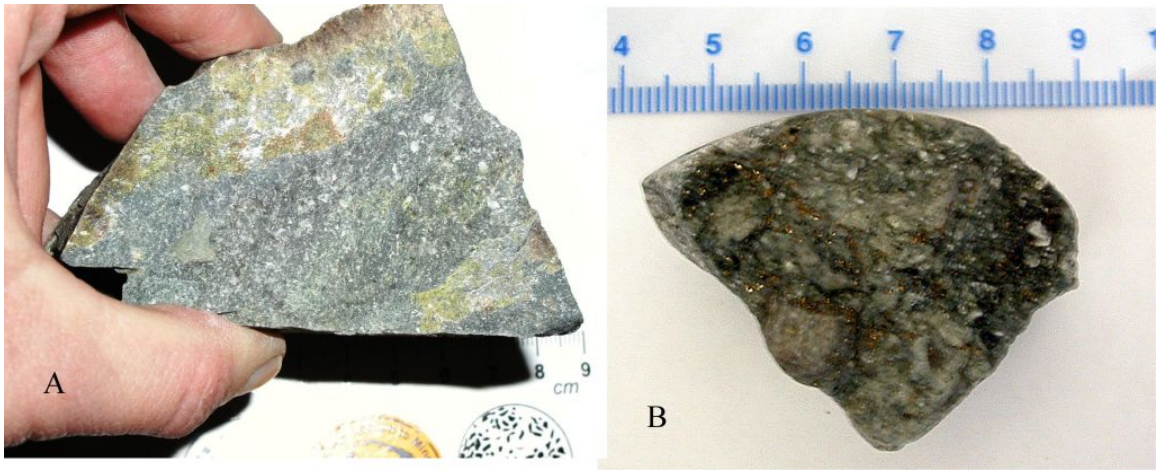

FIGURE 38. (A) Sample ROC-VTM-G021 is greenish gray, finely porphyritic andesite of the Latir volcanics with epidote alteration. (B) Sample PIT-VCV-0009 is propylitically-altered porphyritic andesite with disseminated pyrite.

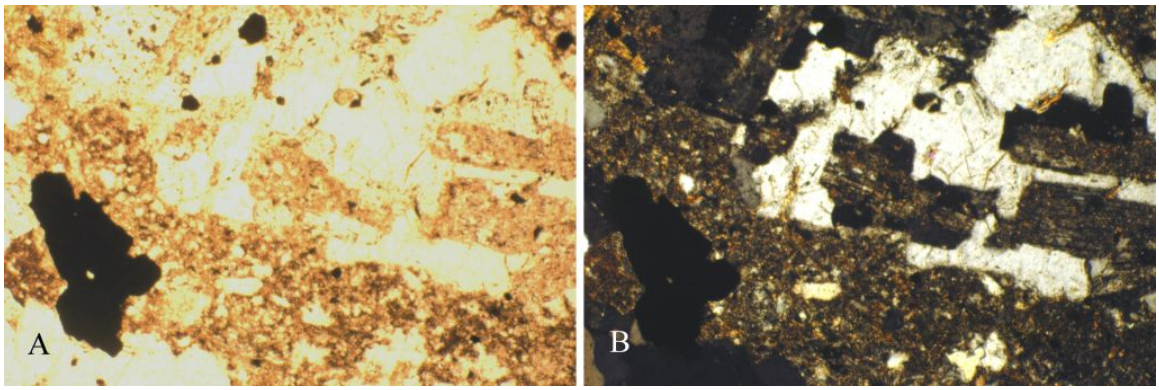

FIGURE 39. Thin section of sample PIT-VCV-0009, andesite, under normal plane polarized light (A) and crossed polarized light (B) showing quartz, feldspar, and pyrite grains in a fine-grained groundmass. Magnification is 5 times and field of view is approximately 1.8 mm.

FIGURE 40. (A) Sample ROC-VTM-G025 shows a vein of quartz-pyrite-sericite (QSP alteration) cutting andesite of the Latir volcanics. (B) Sample PIT-KMD-0007 is QSP-

hydrothermally-altered andesite with finely disseminated pyrite and quartz-molybdenum-pyrite veining.

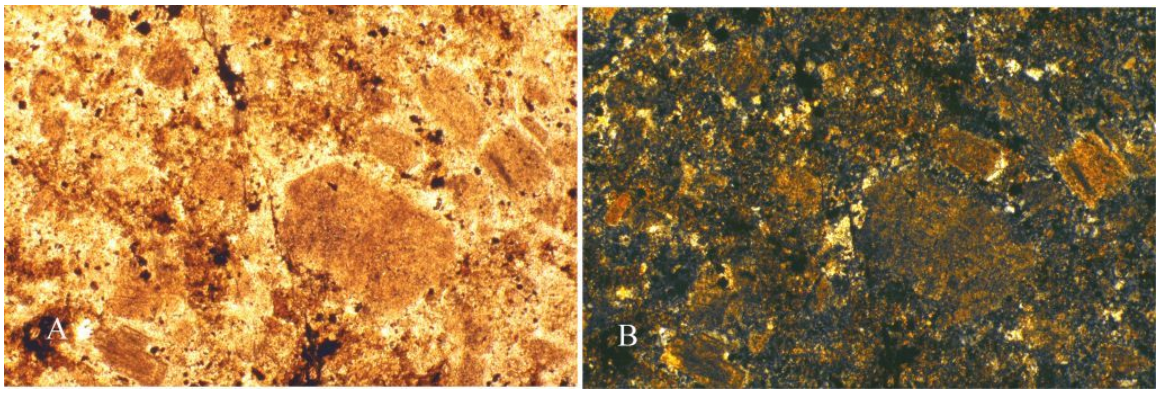

FIGURE 41. Thin section photographs of sample PIT-KMD-0007, andesite, under normal plane polarized light (A) and crossed polarized light (B) showing highly altered feldspar phenocrysts replaced by illite and with chlorite (green) and other clay minerals. Magnification is 5 times and field of view is approximately 1.8 mm.

Fine-grained andesite

The fine-grained andesite contains as much as 30% (5 mm) euhedral plagioclase, 1-8% (1-5 mm) euhedral biotite, 1-10% (2-8 mm) euhedral hornblende, and 0-5% (1-3 mm) subhedral quartz (Figs. 42). It is found as extensive flows up to 200 ft thick and as minor dikes and sills.

FIGURE 42. Sample ROC-VTM-G023 is greenish-gray, propylitic-altered, fine-grained andesite of the Latir volcanics. Pyrite-filled fractures cut the andesite.

Quartz latite

The quartz latite is porphyritic to fine grained and contains as much as 25% (5 mm) euhedral plagioclase, 1-8% (1-5 mm) euhedral biotite, 1-10% (2-8 mm) euhedral hornblende, and 5-10% (1-3 mm) subhedral quartz (Figs. 43-44). It is found as extensive flows up to 200 ft thick and as minor dikes and sills.

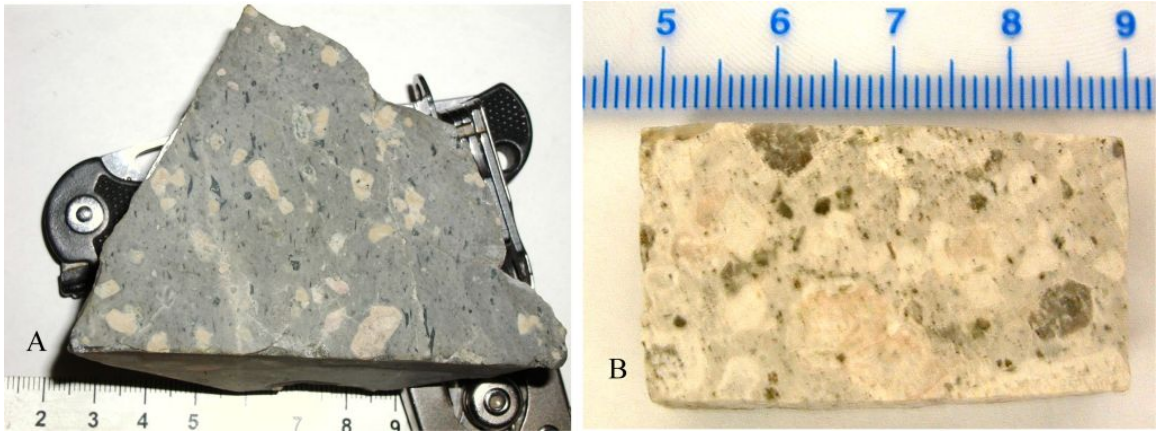

FIGURE 43. (A) Sample ROC-VTM-G013 is gray quartz latite flow of the Latir volcanics with feldspar, quartz, hornblende phenocrysts. (B) Sample GMG-PIT-0009 is white-gray hydrothermal-altered quartz latite porphyry with pink and white feldspar phenocrysts.

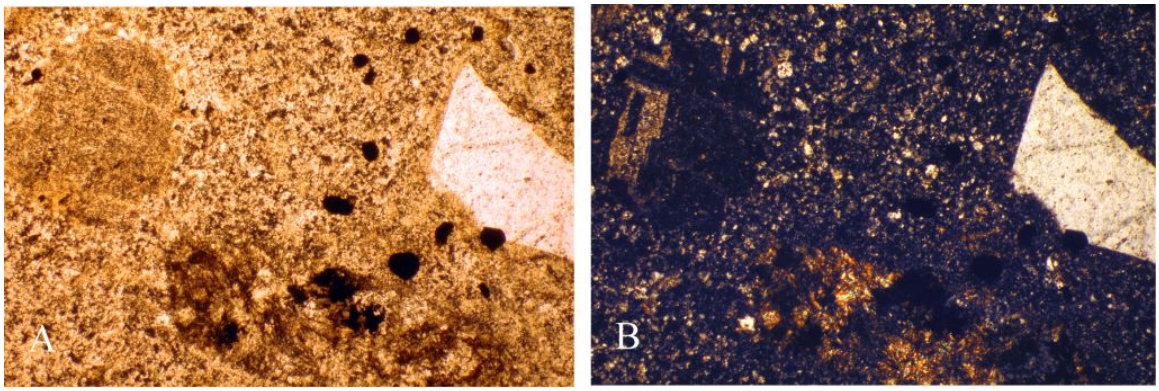

FIGURE 44. Thin section photographs of sample GMG-PIT-0009, andesite, under normal plane polarized light (A) and crossed polarized light (B) showing quartz and feldspar phenocrysts with a hydrothermally altered mica grain, now chlorite, in a fine-grained hydrothermally altered groundmass. Magnification is 5 times and field of view is approximately 1.8 mm.

Fine-grained, porphyritic andesite

The fine-grained, porphyritic andesite consists of 50-70% (0.5-2 mm) subhedral plagioclase laths (Fig. 45-46).

FIGURE 45. Sample ROC-VTM-G022 is fine-grained, porphyritic andesite of the Latir volcanics. Porphyritic texture with small phenocrysts of feldspar and disseminated pyrite.

FIGURE 46. Sample ROC-VTM-G031 is fine-grained, porphyritic andesite of the Latir volcanics showing phyllic alteration overprinted by QSP alteration.

Biotitized andesite

One stage of the hydrothermal alteration produces biotite in the altered andesite and is shown in Figure 47.

FIGURE 47. Sample ROC-VTM-G014 is fine-grained black andesite of the Latir volcanics containing pyrite and showing biotitization.

Andesite breccia

Andesite flow breccias include poorly-sorted andesite fragments of all types of andesite in fragmental, purple to gray to green matrix (Fig. 48-51). Matrix contains sparse fragmental quartz crystals and can be latitic in composition. It forms as upper units of the andesitic volcanic sequence, and is locally interbedded with rhyolite flows. It is typically greenish gray due to epidote and chlorite alteration and is locally called watermelon breccia.

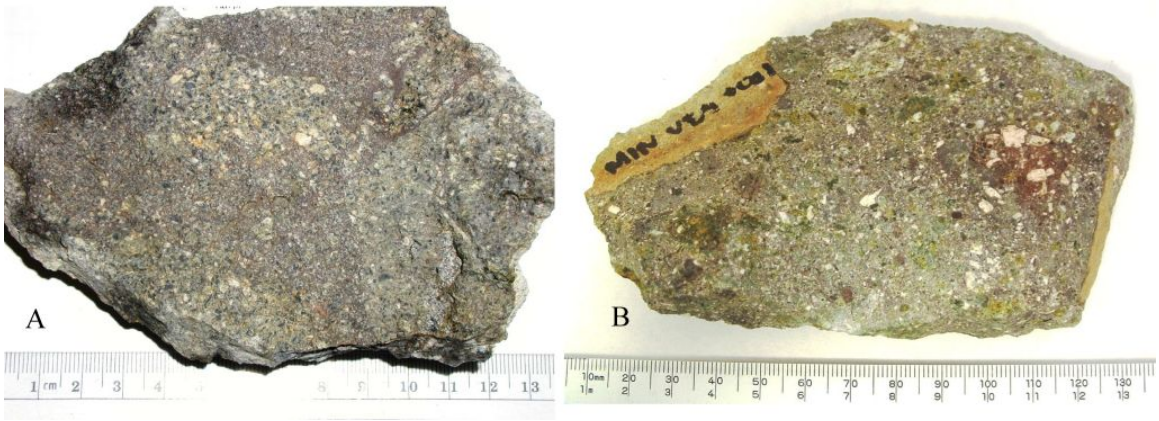

FIGURE 48. (A) Sample ROC-VTM-G029 is andesite breccia of the Latir volcanics, locally called watermelon breccia. (B) Sample MIN-VTM-0001 is hand sample of watermelon breccia.

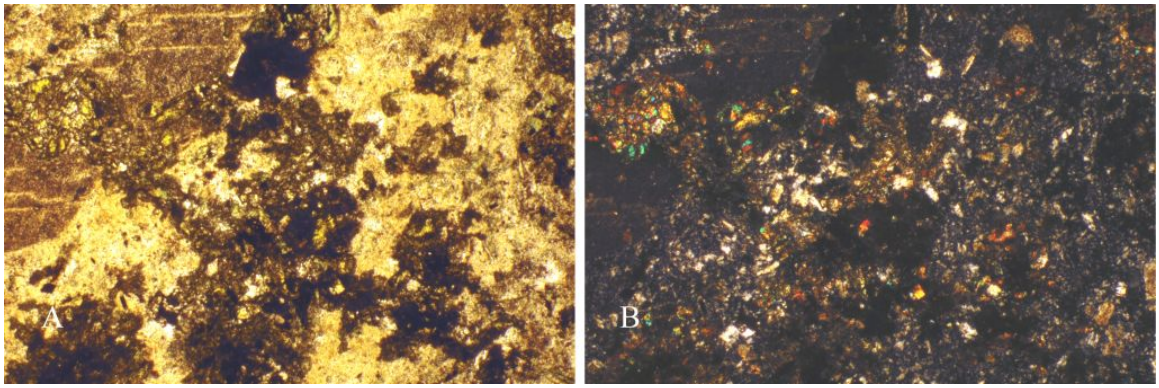

FIGURE 49. Thin section photographs of sample MIN-VTM-0001, andesite, under normal plane polarized light (A) and crossed polarized light (B) showing chlorite (green to brown) and altered feldspars replaced by illite (cream colored). Magnification is 5 times and field of view is approximately 1.8 mm.

FIGURE 50. Sample ROC-VTM-G028 is andesite breccia of the Latir volcanics.

FIGURE 51. Sample ROC-VTM-G024 is greenish-gray to purplish-gray andesite breccia of the Latir volcanics with propylitic alteration. Pyrite mineralized clasts are outlined.

Volcaniclastic rocks

Minor sandstones, siltstone, shales, and volcanic breccias are interbedded with the andesite and latite flows of the Latir volcanics (Figs. 52-53). These volcaniclastic rocks, if hydrothermally altered, are difficult to distinguish from altered andesite and latite flows.

FIGURE 52. Photograph of sample GHR-VWL-0006-T002 is a hydrothermally altered, matrix-supported sandstone.

FIGURE 53. Photograph of sample GHR-VWL-00011-T002 is a hydrothermally altered, fine-grained sandstone.

CHEMICAL CHARACTERIZATION OF THE LITHOLOGIES AND ALTERATION ASSEMBLAGES AT QUESTA

The average range in mineralogical compositions of relatively unaltered lithologies in the Questa-Red River area are listed in Table 7, obtained from petrographic analysis performed in this study and from published literature (Lipman and Read, 1989; Molling, 1989; Meyer, 1991). The average whole-rock chemical compositions of relatively unweathered volcanic and intrusive rocks (including various hydrothermally-altered rocks) in the Questa-Red River area are listed in Table 8, obtained from published literature and this project (Lipman and Read, 1989; Molling, 1989; Meyer, 1991). Mineralogical and chemical compositions of relatively unweathered volcanic and intrusive rocks (including various hydrothermally-altered rocks) in the Questa-Red River area are in Appendix 1.

Chemically, the volcanic rocks in the Questa-Red River area are calc-alkaline, metaluminous to peraluminous igneous rocks (Fig. 54). In general, the volcanic rocks plot in appropriate fields identified as andesite, rhyodacite, and rhyolite on typical litho-geochemical classification diagrams (Fig. 55). The rhyolite (Amalia Tuff) has more quartz and little to no epidote and chlorite compared to the andesite. The rhyolite typically has higher SiO_2, K_2O, Rb, Nb, less TiO_2, Al_2O_3, Fe_2O_3T, MgO, CaO, P_2O_5, and Sr than the andesite.

TABLE 7. Average range in modal mineralogical compositions in weight percent of relatively unweathered major volcanic and intrusive rocks at the Questa mine (Lipman and Read, 1989; Molling, 1989; Meyer, 1991; and petrographic analyses by E.H. Phillps, D. Sweeney, V.T. McLemore). Tr=trace

	Andesite (%)	Quartz Latite (%)	Amalia Tuff (rhyolite) (%)	Goathill Porphyry (%)	Aplite porphyry (%)
Quartz	0-5	tr-10	4-5	1-10	0-2
Plagioclase	30-50	10-30	0-2	4-10	4-8
K-feldspar	0-10	3-8	4-7	2-10	2-6
Hornblende	tr-10	1-10	0	0	Tr-6
Biotite	tr-8	1-8	0	Tr-2	4-8

	Andesite (%)	Quartz Latite (%)	Amalia Tuff (rhyolite) (%)	Goathill Porphyry (%)	Aplite porphyry (%)
Clinopyroxene	tr-2	1-2		0	0
Magnetite	0-5	0-5			
Pumice			20-30		
Rock fragments	0-10	0-10	0-5		
Groundmass	10-90	10-90	30-80	10-50	10-50

TABLE 8. Chemical composition of relatively unweathered volcanic and intrusive rocks (including various hydrothermally-altered rocks) from the Questa-Red River area (from Dillet and Czamanske, 1987; Lipman, 1988; Johnson et al., 1989; P. Lipman, written communication, 2007, and project data). Major oxides in percent and trace elements in parts per million (ppm).

Lithology	Average andesite (standard deviation) N=49	Average quartz latite (standard deviation) N=5	Average Amalia Tuff (standard deviation) N=18	Average granitic intrusions (standard deviation) N=31
SiO_2	62.17 (5.0)	65.38 (1.2)	74.78 (5.5)	71.27 (4.6)
TiO_2	0.65 (0.16)	0.66 (0.1)	0.23 (.2)	0.36 (0.2)
Al_2O_3	14.88 (1.7)	15.42 (0.4)	12.44 (!.7)	13.40 (1.3)
FeOT	4.49 (1.6)	4.60 (0.4)	1.94 (1.7)	1.96 (1.4)
MnO	0.10 (0.05)	0.07 (0.01)	0.05 (0.04)	0.06 (0.04)
MgO	2.09 (1.3)	2.25 (0.09)	0.4 (0.5)	0.81 (0.8)
CaO	2.83 (1.5)	4.05 (0.15)	0.42 (0.5)	1.93 (4.9)
Na_2O	2.33 (1.4)	3.95 (0.3)	2.32 (1.6)	3.38 (1.3)
K_2O	3.99 (1.0)	3.19 (0.5)	4.89 (0.9)	4.53 (1.2)
P_2O_5	0.27 (0.1)	0.33 (0.1)	0.06 (0.09)	0.11 (0.09)
LOI	4.4 (2.2)	1.16 (1.3)	2.11 (1.7)	1.77 (1.8)
Ba	1064 (400)	1293 (138)	344 (373)	575 (461)
Rb	130 (316)	78 (39)	145 (24)	203 (358)
Sr	465 (316)	880 (190)	43 (71)	202 (191)
Pb	29 (36)	23 (2)	47 (58)	24 (14)
Th	9 (4)	9 (2)	14 (4)	17 (8)
U	2 (1)	3 (1)	5 (1)	5 (3)
Zr	175	148	283	179

Lithology	Average andesite (standard deviation) N=49	Average quartz latite (standard deviation) N=5	Average Amalia Tuff (standard deviation) N=18	Average granitic intrusions (standard deviation) N=31
	(29)	(30)	(77)	(92)
Nb	13 (6)	11 (5)	33 (7)	26 (10)
Y	20 (9)	16 (6)	47 (22)	20 (15)
V	96 (37)	71 (5)	26 (34)	32 (31)
Ni	38 (31)	29 (3)	9 (18)	8 (12)
Cu	70 (70)	19 (9)	61 (124)	56 (106)
Zn	81 (80)	63 (6)	22 (4)	55 (53)
Cr	82 (71)	46 (6)	11 (21)	18 (33)
F	1891 (1805)		1193 (797)	1415 (1134)
La	41 (8)		41 (22)	38 (11)
Ce	78 (15)		80 (44)	68 (22)
Nd	32 (8)		34 (19)	24 (12)

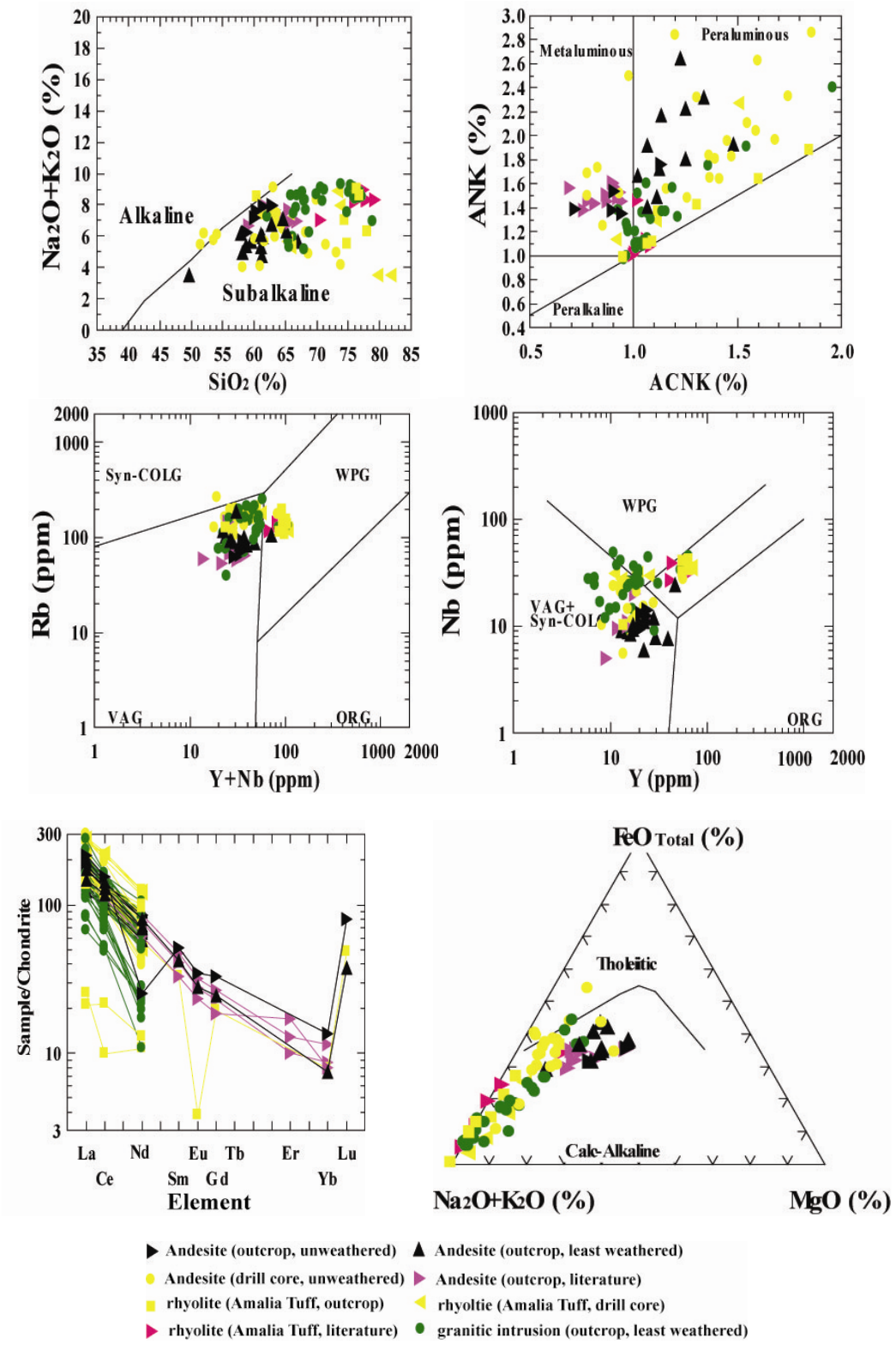

FIGURE 54. Lithogeochemical classification plots of relatively unweathered volcanic and intrusive rocks (including various hydrothermally-altered rocks) for the Questa-Red

River area. Chemical analyses are in the Appendix 1. ANK=Al_2O_3+Na_2O+K_2O. ACNK=Al_2O_3+CaO+ Na_2O+K_2O.

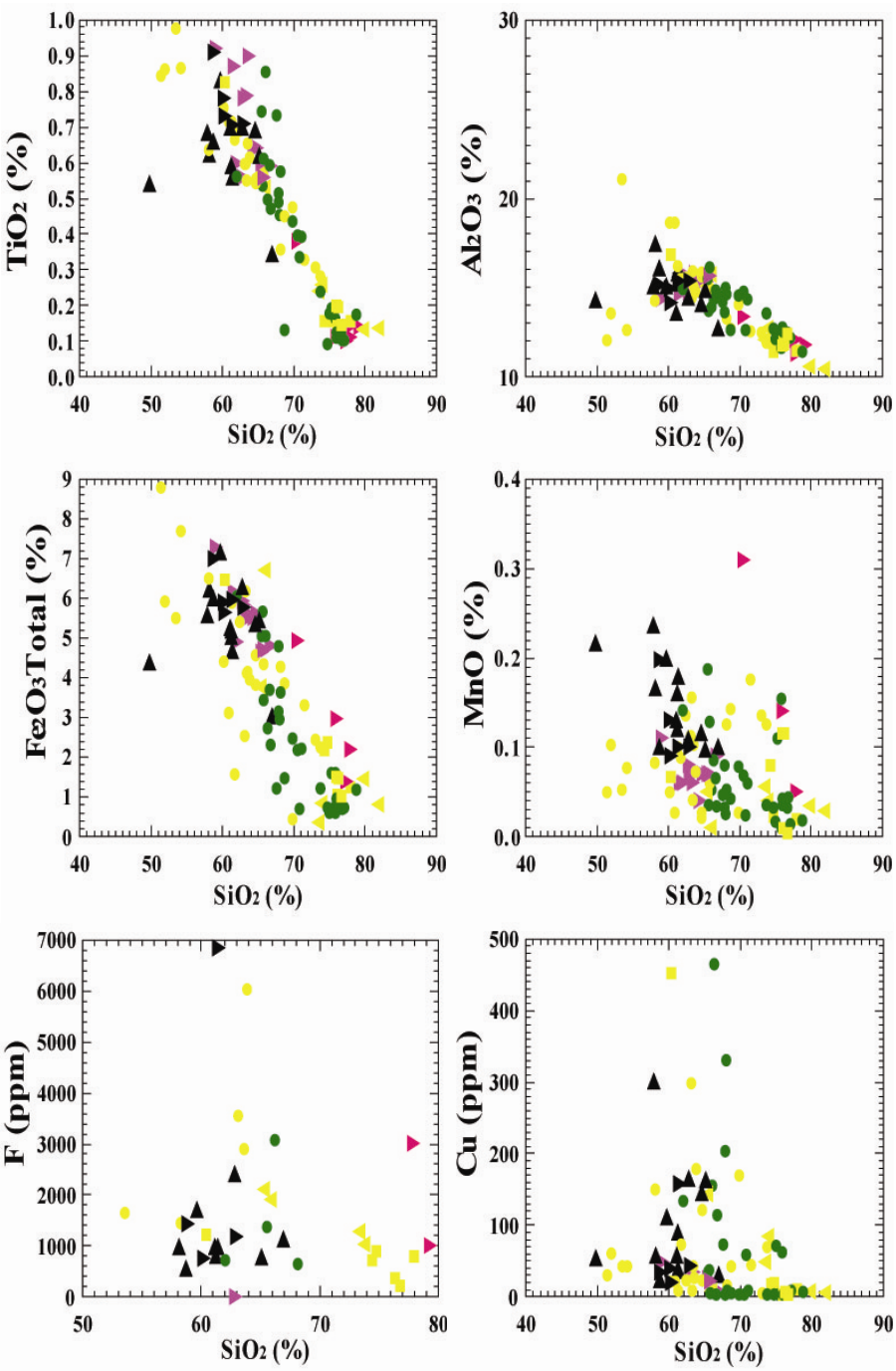

FIGURE 55. Scatter plots of selected elements and SiO_2 of relatively unweathered volcanic and intrusive rocks (including various hydrothermally-altered rocks) for the Questa-Red River area. Chemical analyses are in Appendix 1. Key is in Figure 54.

Figure 56 shows the Questa-Red River fresh, relatively unweathered volcanic and intrusive rocks (including various hydrothermally-altered rocks) in terms of alteration

filter diagrams showing unaltered and hydrothermally altered fields (after Wilt, 1995; Keith and Swan, 1996; McLemore et al., 1999). Many of the drill-core samples show little chemical effect of the hydrothermal alteration, whereas a few of the fresh, unaltered samples plot in the alteration fields. This figure shows the complexity of pre-mining hydrothermal alteration effects on the chemistry and mineralogy of unaltered samples.

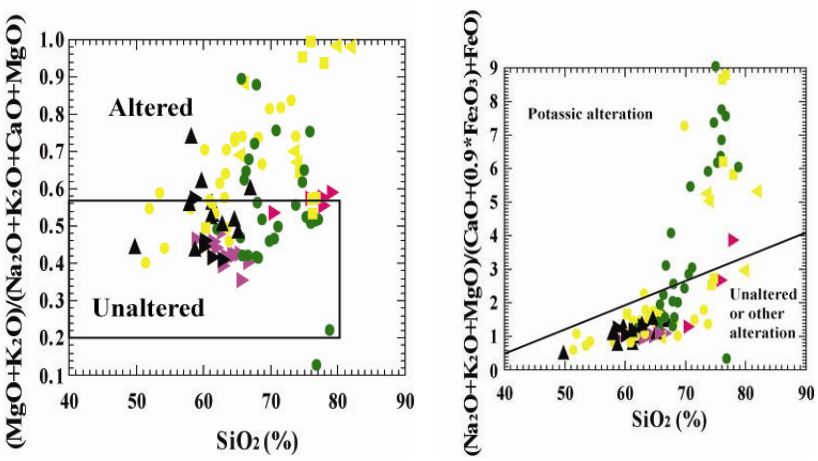

FIGURE 56. Graphs of relatively unweathered volcanic and intrusive rocks (including various hydrothermally-altered rocks) using alteration filter diagrams showing unaltered and hydrothermally altered fields (after Wilt, 1995; Keith and Swan, 1996; McLemore et al., 1999). Chemical analyses are in the project database. Major element oxides are in weight percent and trace elements are in parts per million (ppm). Key is in Figure 54.

PARAGENESIS OF HYDROTHERMAL ALTERATION

Paragenesis is the sequence of hydrothermal events and is determined by detailed petrographic descriptions. Previous workers have described various aspects of the paragenesis of the hydrothermal alteration in the Questa deposit (Carpenter, 1968; Schilling, 1956; Bloom, 1981; Molling, 1983) and these results are summarized in Table 9 and Figures 57-59.

TABLE 9. Comparison of paragenesis of the vein and breccia deposits by different workers. q=quartz, b=biotite, K-K-feldspar, mo=molybdenite, f=fluorite, ru=rutile, py=pyrite, cc=calcite, cp=chalcopyrite, sp=sphalerite, gn=galena, rh=rhodocrosite, gy=gypsum, mh=malachite, lm=limonite, s=sericite. Ross et al. (2002) describes the paragenesis only of the main MHBx mineralizing event.

Stage	Molling (1968)	Bloom (1981)	Schilling (1956)	Carpenter (1968)	Ross et al. (2002)
1-early	q	q	q	q	
2	q-b-K-mo±f, ru	q-b-K±mo	b-q-mo	q-mo-py-K; b-K-q	b, K, q±mo
3	q-mo±py	q-mo	q-mo	q-mo-py-f-cc	b, K, q±mo
4	f-q (cc)		f		b, q, K, mo
5	q±mo±py				b, q, K, mo
6	py-q±mo	q-py±mo	py		b, q, s, phl, K, cc, mo±f
7	mo±q±p				q, phl, cc, mo, s, b±f

Stage	Molling (1968)	Bloom (1981)	Schilling (1956)	Carpenter (1968)	Ross et al. (2002)
8	Py-q (cp-sp-gn)	q-py-cp-sp-gn	Py-cp-sp-gn		q, phl, cc, mo, s±f
9	f-q±py		f	rh-f-cc-gn-cp	
10	q-cc				
11	rh-cc			cc-rh	
12	gy±mo			mo	mo-q±cc±f
13	mh		Lm-mh-fm		

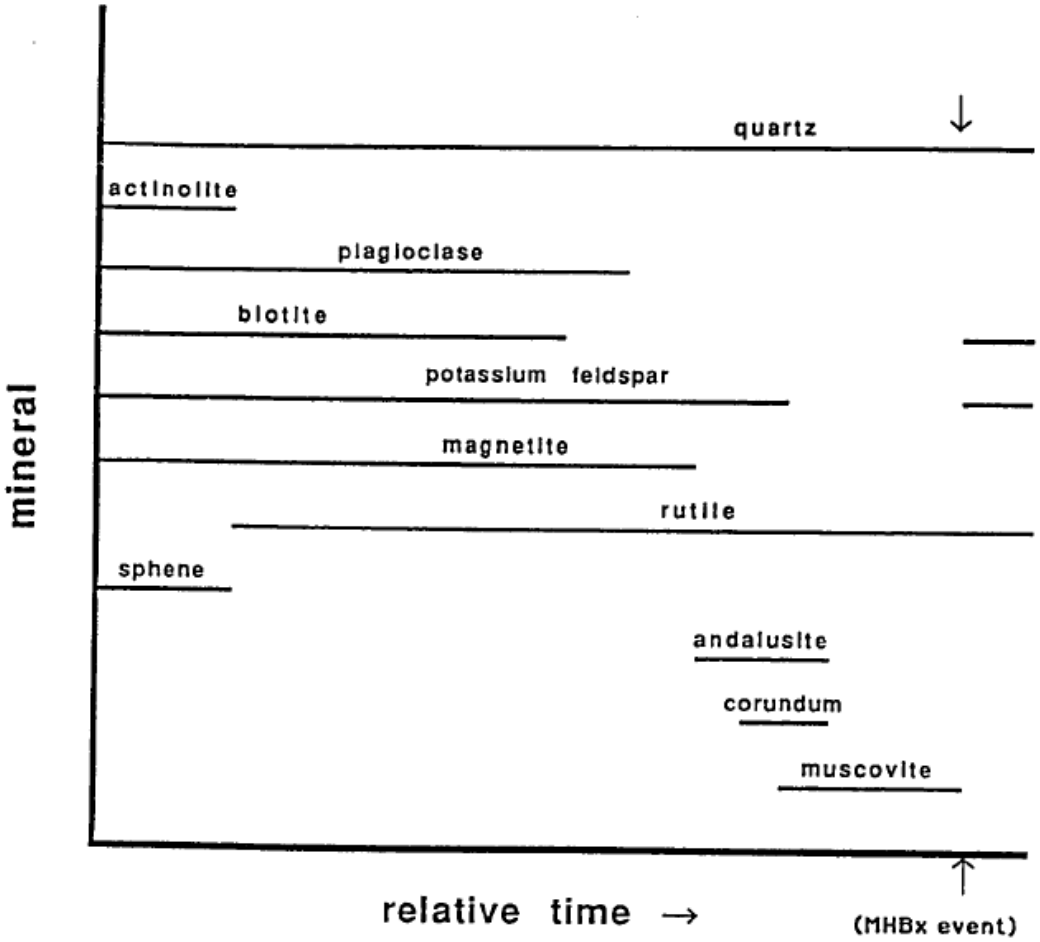

FIGURE 57. General paragenesis of mineralization and alteration (from Molling, 1968). MHBx event is the main mineralizing event, which is described in detail by Ross et al. (2002) in Table 9 and Figure 58.

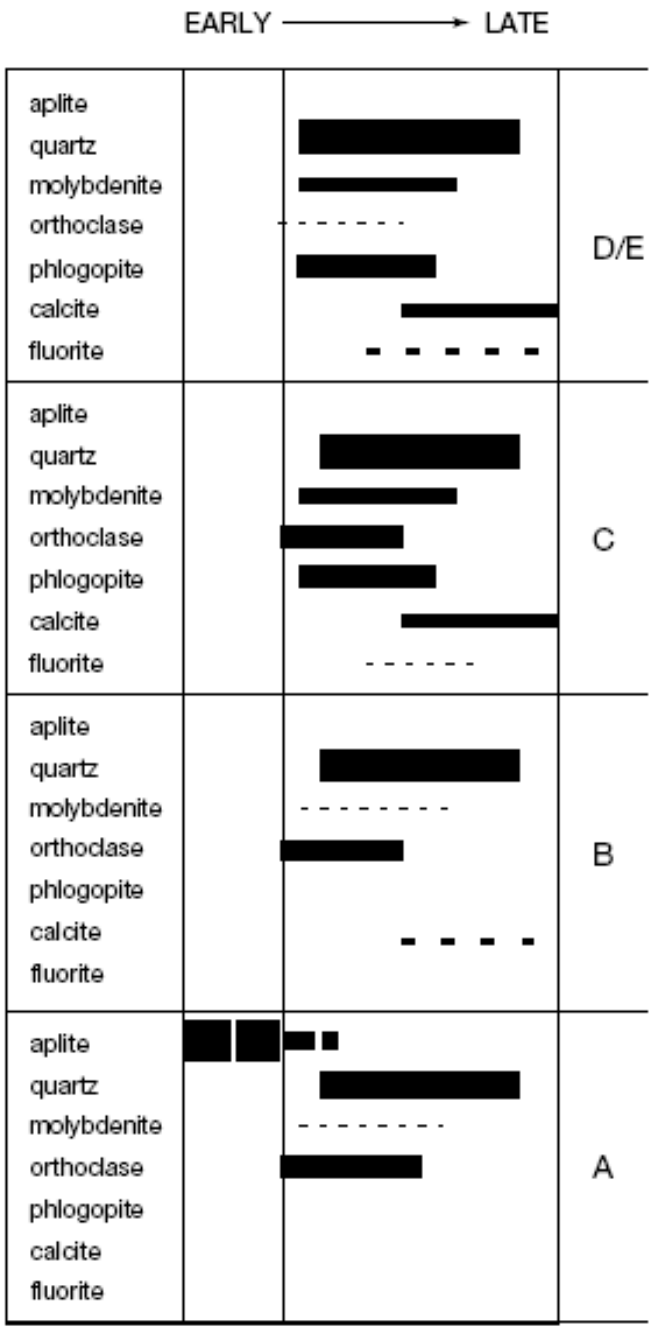

FIGURE 58. Paragenesis of the Questa breccia ore deposit (from Ross et al., 2002). A-E represents the different breccia facies.

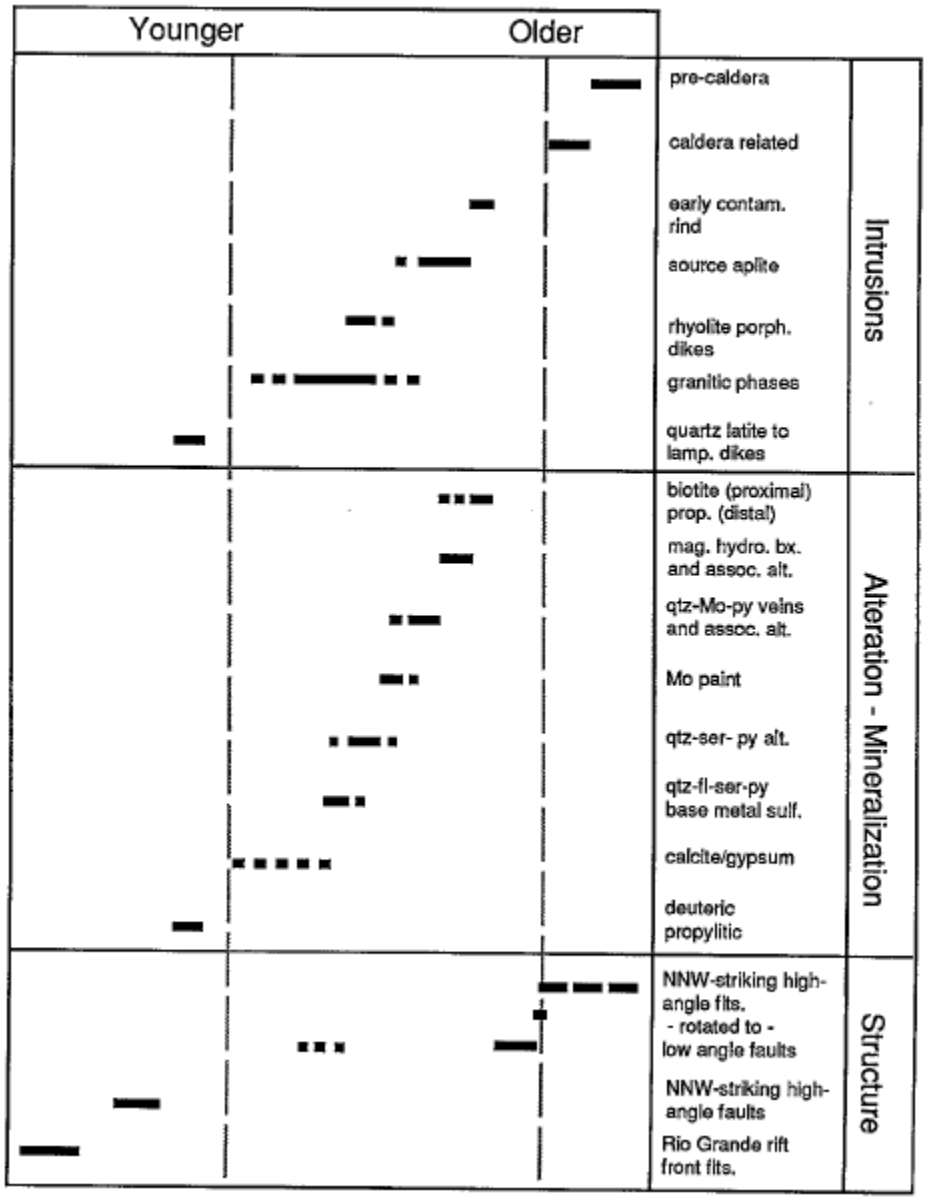

FIGURE 59. Paragenesis of the Questa mineral deposit and alteration (from Meyer and Leonardson, 1990).

SUMMARY

- Chemically, the volcanic rocks in the Questa-Red River area are calc-alkaline, metaluminous to peraluminous igneous rocks.
- The rhyolite (Amalia Tuff) has more quartz and little to no epidote and chlorite compared to the andesite.
- The rhyolite (Amalia Tuff) typically has higher SiO_2, K_2O, Rb, Nb, less TiO_2, Al_2O_3, Fe_2O_3T, MgO, CaO, P_2O_5, and Sr than the andesite.
- Little, if any, unaltered rocks (i.e. primary magmatic) went into the Questa rock piles.

- The rock pile samples are a mixture of two or more rock types that were variably hydrothermally altered. GHN is a mixture of rhyolite (Amalia Tuff) and andesite.
- The rocks that went into the Questa rock piles were hydrothermally altered before mining, which resulted in large variations in mineralogical and chemical composition.
    - Amphiboles, pyroxenes, and feldspars were replaced by biotite and albite during alteration.
    - Biotite, hornblende, pyroxenes were hydrothermally altered to chlorite, sericite, smectite, illite, and mixed layer clays (prophyllitic alteration).
    - Feldspars show varying degrees of hydrothermal alteration to illite, kaolinite, smectite, quartz, mixed layer clays (QSP overprinting prophyllitic alteration).
    - Many rocks were silicified, and this silicification was accompanied by the addition of 1-2 stages of pyrite, illite, calcite, and/or gypsum.

REFERENCES

Bauer, P.W., Kelson, K.I., and Koning, D.J., 2004, Plate 7: Cenozoic geologic timeline—Taos area: New Mexico Geological Society Guidebook, 55, p. 122.

Bloom, M.S., 1977, Chemistry of inclusion fluids; stockwork molybdenum deposits from Questa, New Mexico, Hudson Bay Mountain, and Endako, British Columbia: Economic Geology, v. 76, p. 1906-1920.

Browne, P.R.L., 1978, Hydrothermal alteration in active geothermal fields: Annual Reviews of Earth and Planetary Science, v. 6, p. 229–250.

Caine, J.S., 2003, Questa Baseline and Pre-Mining Ground-Water Quality Investigation. 6. Preliminary Brittle Structural Geologic Data, Questa Mining District, southern Sangre de Cristo Mountains, New Mexico: U.S. Geological Survey Open-File Report 03-280, http://pubs.usgs.gov/sir/2005/5149/, accessed 11/8/08.

Caine, J.S., 2006, Questa Baseline and Pre-Mining Ground-Water Quality Investigation. 18. Characterization of brittle structures in the Questa caldera and speculation on their potential impacts on the bedrock ground-water flow system, Red River watershed, New Mexico: U.S. Geological Survey Professional Paper 1729, 37 p., http://pubs.usgs.gov/of/2003/ofr-03-280/, accessed 11/8/08.

Carpenter, R.H., 1968, Geology and Ore Deposits of the Questa Molybdenum Mine Area, Taos County, New Mexico: Ore Deposits of the United States, 1933-1967, vol. 2, AIME Graten-Sales, p.1328-1350.

Carten, R.B., White, W.H., and Stein, H.J., 1993, High-grade granite-related molybdenum systems—Classification and origin, *in* Kirkham, R.V., Sinclair, W.D., Thorpe, R.I., and Duke, J.M., eds., Mineral deposit modeling: Geological Association of Canada Special Paper 40, p. 521–554.

Clark, K.F., 1968, Structural controls in the Red River District, New Mexico: Economic Geology, v. 63, p. 553-566.

Czamanske, G.K., Foland, K.A., Hubacher, F.A. and Allen, J.C., 1990, The $^{40}Ar/^{39}Ar$ Chronology of Caldera Formation, Intrusive Activity and Mo-ore Deposition near Questa, New Mexico: New Mexico Geological Society, Guidebook 41, p. 355-358.

Delvigne, J.E., 1998, Atlas of micromorphology of mineral alteration and weathering: Canadian Mineralogist, Special Publication 3, 494 p.

Dillet, B. and Czamanske, G.K., 1987, Aspects of the Petrology, mineralogy, and geochemistry of the granitic rocks associated with Questa Caldera, Northern New Mexico: U.S. Geological Survey, Open-file Report 87-0258, 238 p.

Graf, G.J., 2008, Mineralogical and geochemical changes associated with sulfide and silicate weathering, natural alteration scars, Taos County, New Mexico: M. S. thesis, New Mexico Institute of Mining and Technology, Socorro.

Hall, J.S., 2004, New Mexico Bureau of Mines and Mineral Resource's Clay Laboratory Manual: Unpublished New Mexico Bureau of Geology and Mineral Resources report.

Henley, R.W. and Ellis, A.J., 1983, Geothermal systems, ancient and modern: a geochemical review: Earth Science Reviews, v. 19, p. 1–50.

Johnson, C.M., Czamanske, G.K., and Lipman, P.W., 1989, Geochemistry of intrusive rocks associated with the Latir volcanic field, New Mexico, and contrasts between evolution of plutonic and volcanic rocks: U.S. Geological Survey, Open-file Report 90-109, 103 p.

Keith, S.B. and Swan, M.M., 1996, The great Laramide porphyry copper cluster of Arizona, Sonora, and New Mexico: The tectonic setting, petrology, and genesis of a world class porphyry metal cluster; *in* Coyner, A.R., Fahey, P.L., eds., Geology and Ore Deposits of the American Cordillera: Geological Society of Nevada Symposium Proceedings, Reno, Sparks, Nevada, p. 1667–1747.

Lipman, P.W., 1988, Evolution of silicic magma in the upper crust: the Min-Tertiary Latir Volcanic Field and its cogenetic granitic batholith, northern New Mexico, U.S.A.: Transactions of the Royal Society of Edinburgh, Earth Sciences, v. 79, p. 265-288.

Lipman, P.W. and Reed, J.C., Jr., 1989, Geologic map of the Latir volcanic field and adjacent areas, northern New Mexico: U.S. Geological Survey, Miscellaneous Investigations Map I-1907, scale 1:48,000.

Loucks, T.A., Phillips, J.S., and Newell, R.A., 1977, Exploration potential of the Questa East area: unpublished report for Kennecott Copper Corporation.

Ludington, S.D., 1986, Descriptive model of Climax Mo deposits, *in* Cox, D.P., and Singer, D.A., eds., Mineral deposit models: U.S. Geological Survey Bulletin 1693, p. 73.

Ludington, S.D., Bookstrom, A.A., Kamilli, R.J., Walker, B.M., and Klein, D.P., 1995, Climax Mo deposits, *in* du Bray, E.A., ed., Preliminary compilation of descriptive geoenvironmental mineral deposit models: U.S. Geological Survey, Open-File Report 95-831, p. 70–74.

Ludington, S., Plumlee, G., Caine, J., Bove, D., Holloway, J., and Livo, E., 2005, Questa baseline and pre-mining ground-water quality Investigation, 10. Geologic influences on ground and surface waters in the lower Red River watershed, New Mexico: U.S. Geological Survey, Scientific Investigations Report 2004-5245, 46 p.

Martineau, M.P., Heinemeyer, G.R., Craig, S.D., and McAndrews, K.P., 1977, Geological report: Questa Project 1975-1977: unpublished mine report, Questa Molybdenum Company.

McLemore, V.T., 2009, Geologic Setting and Mining History of the Questa mine, Taos County, New Mexico: New Mexico Bureau of Geology and Mineral Resources, Open-file report OF-515, 29 p. (unpublished report to Molycorp, Inc, Task 1.2.2, B1.1, Revised October 3, 2005, appendix 1.1, May 2005 report, revised August 2008).

McLemore, V.T., Boakye, K., Campbell, A., Donahue, K., Dunbar, N., Gutierrez, L., Heizler, L., Lynn, R., Lueth, V., Osantowski, E., Phillips, E., Shannon, H., Smith, M., Tachie-Menson, S., van Dam, R., Viterbo, V.C., Walsh, P., and Wilson, G.W., 2008a, Characterization of Goathill North Rock Pile: revised unpublished report to Molycorp, Tasks: 1.3.3, 1.3.4, 1.4.2, 1.4.3, 1.11.1.3, 1.11.1.4, 1.11.2.3, B1.1.1, B1.3.2.

McLemore, V.T., Anim, K., Fakhimi, A., Dickens, A.K., and Nunoo, S., 2008b, Characterization of Questa rock piles, New Mexico: Unpublished report to Chevron Mining, Inc and the QRPWASP, Task B1.1.

McLemore, V.T., Donahue. K.M., Phillips, E.H., Dunbar, N., Walsh, P., Guitierrez, L.A.F., Tachie-Menson, S., Shannon, H.R., Lueth, V.W., Campbell, A.R., Wilson, G.W., and Walker, B.M., 2006a, Characterization of Goathill North mine rock pile, Questa molybdenum mine, Questa, New Mexico; in 7th ICARD, March 26-30, 2006, St. Louis MO.: Published by American Society of Mining and Reclamation., Lexington, KY. CD-ROM, p. 1219-1249.

McLemore, V.T., Donahue, K., Phillips, E., Dunbar, N., Smith, M., Tachie-Menson, S., Viterbo, V., Lueth, V.W., Campbell, A.R., and Walker, B.M., 2006b, Petrographic, mineralogical and chemical characterization of Goathill North Mine Rock Pile, Questa Molybdenum Mine, Questa, New Mexico: 2006 Billings Land Reclamation Symposium, June, 2006, Billings, Mt. Published by Published by American Society of Mining and Reclamation, 3134 Montavesta Rd., Lexington, KY, CD-ROM, http://geoinfo.nmt.edu/staff/mclemore/Molycorppapers.htm

McLemore, V.T., Fakhimi, A., van Zyl, D., Ayakwah, G.F., Anim, K., Boakye, K., Ennin, F., Felli, P., Fredlund, D., Gutierrez, L.A.F., Nunoo, S., Tachie-Menson, S., and Viterbo, V.C., 2009a, Literature review of other rock piles: characterization, weathering, and stability: New Mexico Bureau of Geology and Mineral Resources, Open-file report OF-517, 102 p. (unpublished report to Molycorp Management, Task B4.2.5).

McLemore, V.T., Munroe, E.A., Heizler, M.T., and McKee, C., 1999, Geochemistry of the Copper Flat porphyry and associated deposits in the Hillsboro mining district, Sierra County, New Mexico, USA: Journal of Geochemical Exploration, v. 67, p. 167-189.

McLemore, V.T., Sweeney, D., Dunbar, N., Heizler, L. and Phillips, E., 2009b, Determining quantitative mineralogy using a combination of petrographic techniques, whole rock chemistry, and MODAN: Society of Mining, Metallurgy and Exploration Annual Convention, preprint 09-20, 19 p.

Meyer, J.W., 1991, Volcanic, plutonic, tectonic and hydrothermal history of the southern Questa Caldera, New Mexico: University Microfilms, Ph.D. dissertation, 348 p.

Meyer, J.W., and Leonardson, R.W., 1990, Tectonic, hydrothermal and geomorphic controls on alteration scar formation near Questa, New Mexico: New Mexico Geological Society, Guidebook 41, p. 417-422

Molling, P.A., 1989, Applications of the reaction progress variable to hydrothermal alteration associated with the deposition of the Questa molybdenite deposit, NM: PhD dissertation, Johns Hopkins University, 227 p.

Moore, O.M. and Reynolds, R.O., Jr., 1989, X-ray diffraction and the identification and analyses of clay minerals: Oxford University Press, New York, 378 p.

Mutschler, F.E., Wright, E.G., Ludington, S.D., and Abbott, J.T., 1981, Granitic molybdenite systems: Economic Geology, v. 76, p. 874-897.

Neuendorf, K.K.E., Mehl, J.P., Jr., and Jackson, J.A., 2005, Glossary of Geology: American Geological Institute, 5th ed., Alexandria, Virginia, 779 p.

Norwest Corporation, 2004, Goathill North Slide Investigation, Evaluation and Mitigation Report: unpublished report to Molycorp Inc., 99 p., 3 vol.

Paktunc, A.D., 1998, MODAN: An interactive computer program for estimating mineral quantities based on bulk composition: Computers and Geoscience, v. 24, no. 5, p. 425-431.

Paktunc, A.D., 2001, MODAN—A Computer program for estimating mineral quantities based on bulk composition: Windows version. Computers and Geosciences, v. 27, p. 883-886.

Piché, M. and Jébrak, M., 2004, Normative minerals and alteration indices developed for mineral exploration: Journal of Geochemical Exploration, v. 82, p. 59-77.

Plumlee, G.S., Lowers, H., Koenig, A., Ludington, S., 2005, Questa baseline and pre-mining ground-water quality investigation. 13. Mineral microscopy and chemistry of mined and unmined porphyry molybdenum mineralization along the Red River, New Mexico: Implications for ground- and surface-water quality: U.S. Geological Survey Open-File Report 2005-1442..

Reed, M.H., 1997, Hydrothermal alteration and its relationship to ore fluid composition; in Barnes, H.L., ed., Geochemistry of hydrothermal ore deposits: 3rd edition, John Wiley and Sons, New York, New York, p. 303-365.

Reed, J.C., Jr., Lipman, P. W., and Robertson, J. M., 1983, Geologic map of the Latir Peak and Wheeler Peak Wilderness and the Columbine-Hondo Wilderness Study Area, Taos County, New Mexico: U.S. Geological Survey, Miscellaneous Field Studies Map MF-1570-B, scale 1:50,000.

Roberts, T.T., Parkison, G.A., and McLemore, V.T., 1990, Geology of the Red River district, Taos County, New Mexico: New Mexico Geological Society, Guidebook 41, p. 375-380.

Ross, P.S., Jebrak, M., and Walker, B.M., 2002, Discharge of hydrothermal fluids from a magma chamber and concomitant formation of a stratified breccia zone at the Questa porphyry molybdenum deposit, New Mexico: Economic Geology, v. 97, p. 1679-1699.

Samuels, K.E., 2008, Weathering and landscape evolution recorded in supergene jarosite, Red River valley, northern New Mexico: M.S. thesis, New Mexico Institute of Mining and Technology, Socorro, 171 p.

Schilling, J.H., 1956, Geology of the Questa molybdenum (moly) mine area, Taos County, New Mexico: New Mexico Bureau of Mines and Mineral Resources, Bulletin 51, 87 p.

Shum, M. G. W., 1999, Characterization and dissolution of secondary weathering products from the Gibraltar mine site: M.S. thesis, University of British Columbia, Vancouver, 310 p.

URS Corporation, 2003, Mine rock pile erosion and stability evaluations, Questa mine: Unpublished Report to Molycorp, Inc. 4 volumes.

Van der Plas, D. and Tobi, A.C., 1965, A chart for judging the reliability of point counting results: American Journal of Science, v. 263, p. 87-90.

Westra, G., and Keith, S.B., 1981, Classification and genesis of stockwork molybdenum deposits: Economic Geology, v. 76, p. 844–873.

Wilt, J.C., 1995. Correspondence of alkalinity and ferric=ferrous ratios of igneous rocks associated with various types of porphyry-copper deposits; *in* Pierce, F.W., Bolm, J.G., Eds., Porphyry-Copper Deposits of the America Cordillera: Ariz. Geol. Soc. Digest 20, p. 180–200.

Zimmerer, M.J., 2008, The $^{40}Ar/^{39}Ar$ geochronology and thermochronology of the Latir volcanic field and associated intrusions: Implications for caldera-related magmatism: M.S. thesis, New Mexico Institute of Mining and Technology, Socorro, 119 p.

APPENDIX 1. COMPOSITION OF VOLCANIC AND INTRUSIVE ROCKS IN THE QUESTA-RED RIVER AREA

TABLE A1-1. Chemical composition of relatively unweathered, unaltered andesites from the Questa-Red River area obtained from Dillet and Czamanske (1987), Lipman (1988), Johnson et al. (1989) and P. Lipman, written communication (2007). Major oxides are in weight percent and trace elements in parts per million (ppm).

Sample	110	113	119	1830	1831	1832	78L-187
description	Hornblende andesite	Augite andesite	Augite andesite	Fresh andesite	Fresh andesite	Fresh andesite	Andesite
SiO_2	59.1	63.1	63.4	64.4	62	62.89	61.6
TiO_2	0.92	0.78	0.79	0.65	0.6	0.56	0.87
Al_2O_3	14.4	15.4	15.3	15.23	15.8	14.71	14.7
Fe_2O_3T	7.3	5.83	5.64	5.53	4.92	5.92	6.16
MnO	0.11	0.07	0.06	0.04	0.06	0.08	0.06
MgO	5.44	2.15	2.82	1.91	1.7	2.69	3.9
CaO	6.37	5.05	4.5	3.48	3.55	3.01	4.8
Na_2O	3.53	3.97	4.17	3.8	3.8	3.75	4.1
K_2O	3.11	3.75	3.49	3.45	4.1	3.65	3.6
P_2O_5	0.43	0.38	0.37	0.34	0.37	0.38	0.43
S				0.01	0.01	0.01	
SO_4							
C							
LOI	1.57	2.65	2.29	2.2	2.5	2.89	1.3
Total	102.28	103.13	102.83	101.04	99.41	100.54	101.52
Ba	1180	1135	1330				
Rb	58	81	68				70
Sr	880	855	935				1070
Pb	20	18	21				
Th	10	11	10				6
U	2	3	4				3
Zr	184	177	184				174
Nb	12	11	11				10
Y	19	15	15				18
Sc							
V	125	77	91				
Ni	105	72	67				
Cu	49	33	34				
Zn	81	65	71				
Ga							
Cr	208	125	125				
Co							
F						0.069	
Be							
La							
Ce	92.99	80.8					
Nd	40.21	35.7					

TABLE A1-2. Chemical composition of relatively unweathered andesites (including various hydrothermally-altered rocks) from the Questa-Red River area obtained from this study. SWI=Simple Weathering Index define in McLemore et al. (2008a); a SWI ≤ is fresh (unweathered) to least weathered. Major oxides are in weight percent and trace elements in parts per million (ppm).

Sample	GHN-EHP-0007	GHN-VTM-0504	GHN-VTM-0554	GHN-VTM-0555	GHN-VTM-0604	GHN-VTM-0610	GMG-PIT-0001
description	andesite	andesite	andesite	andesite	andesite	andesite	andesite
SWI	2	2	2	2	2	2	1
SiO_2	58.15	61.18	49.69	61.26	61.375	66.93	53.65
TiO_2	0.624	0.59	0.54	0.59	0.56	0.345	0.97
Al_2O_3	17.43	15.8	14.31	15.24	16.04	12.76	20.96
Fe_2O_3T	6.237	5.2	4.4	5.04	4.67	3.047	5.45
MnO	0.166	0.16	0.217	0.12	0.18	0.101	0.05
MgO	2.31	2.58	1.93	1.99	2.08	0.98	0.28
CaO	0.77	2.75	6.58	3.69	3.72	1.72	3.66
Na_2O	1.3	1.87	0.07	1.17	1.75	1.62	0.34
K_2O	3.68	3.44	3.44	3.54	4.18	4.07	5.3
P_2O_5	0.271	0.2	0.221	0.24	0.19	0.107	0.15
S					0.01	0.02	
SO_4					0.05	0.91	
C			0.01		0.57	0.13	
LOI	7.13	5.15	9.21	6.1	4.77	5.78	5.19
Total					100.15	98.52	
Ba	700	564	645	1432	2960	853	862
Rb	101	89	90	86.9	102	105	199
Sr	149	202	123	225.8	438	101	1004
Pb	38	11	14	13.5	16	27	13
Th	7	6	8	7.5	7	11	6.76
U	4	0	3	1.5	1	5	0.3
Zr	155	158	134	145.5	147	216	222
Nb	7.9	8.5	6	7.7	8.8	24.3	16
Y	29	16	22	39.5	15	47	28.3
Sc	11	11	11	12.5	11	5	
V	105	87	69	106.2	84	45	189
Ni	42	34	54	25.1	34	14	22
Cu	58	38	54	89.7	36	30	40
Zn	321	122	367	104.8	100	249	6
Ga	20	19	19	17.7	19	22	17.5
Cr	50	42	53	38.2	40	26	61
Co							16
F	982	811.5			982	1125	1608
Be	4.4					2.3	
La	37	34	29	36.5	31	32	
Ce	77	64	58	63.9	58	60	
Nd	34	31	30	31	26	28	

Sample	GMG-PIT-0010	MIN-VTM-0018	MIN-VTM-0019	PIT-KMD-0007	PIT-KMD-0008	PIT-KMD-0009	PIT-VCV-0001
description	Andesite breccia	andesite	andesite	QSP-altered andesite	argillic-altered andesite	andesite	andesite
SWI	1	2	1	1	1	1	1
SiO_2	58.33	59.62	58.84	63.27	63.96	63.74	62.64

Sample	GMG-PIT-0010	MIN-VTM-0018	MIN-VTM-0019	PIT-KMD-0007	PIT-KMD-0008	PIT-KMD-0009	PIT-VCV-0001
TiO_2	0.63	0.83	0.91	0.59	0.61	0.65	0.686
Al_2O_3	14.2	15.12	15.19	14.32	14.69	14.98	15.49
Fe_2O_3T	6.45	7.16	6.996	2.5	3.92	4.1	5.346
MnO	0.08	0.2	0.198	0.11	0.07	0.1	0.134
MgO	3.49	4.77	5.2	2.39	1.79	2.39	0.9
CaO	3.73	1.3	2.65	2.85	1.71	3.37	1.02
Na_2O	1.37	3.1	3.33	3.26	3.89	3.35	2.62
K_2O	2.55	2.54	2.89	5.76	2.89	4.06	4.75
P_2O_5	0.19	0.37	0.42	0.18	0.04	0.24	0.337
S		0.03	0.06				4.43
SO_4		0.03					0.05
C		0.07					0.15
LOI	5.73	5.14	2.65	2.44	4.17	3	4.91
Total		100.28					103.46
Ba	864	1132	1223	1333	1404	1237	1054
Rb	123	79	66	186	130	121	151
Sr	488	415	696	496	282	637	165
Pb	146.3	20	9	44.2	46.1	26.3	31
Th	7.74	5.5	7	7.52	5.29	6.97	10
U	1.64	2	1	0.97	1.79	1.77	3
Zr	132	181	186	176	228	145	171
Nb	10	12	11.1	11	15	14	12.2
Y	8.4	23	23	17.2	22.5	15.5	19
Sc		14	16				11
V	126	131	142	116	161	102	103
Ni	36	87	80	12	100	0	10
Cu	147	111	35	295	175	23	20
Zn	117	132	127	67	119	67	41
Ga	20.6	20	20	16.6	20.6	17.8	21
Cr	83	134	151	89	401	76	44
Co	20			31	34	60	
F	1397	1708	1433	3515	6004	2865	
Be							
La		44	43				38
Ce		84	85				78
Nd		42	40				34

Sample	PIT-VCV-0002	PIT-VCV-0003	PIT-VCV-0007	PIT-VCV-0008	PIT-VCV-0009	PIT-VCV-0012	PIT-VCV-0013
description	andesite	andesite	andesite	andesite	andesite	andesite	andesite
SWI	1	1	1	1	1	1	1
SiO_2	68.37	61.44	66	68.84	63.49	71.65	73.97
TiO_2	0.352	0.708	0.56	0.443	0.591	0.324	0.278
Al_2O_3	13.16	16.07	14.88	12.56	14.29	12.45	11.81
Fe_2O_3T	4.235	5.83	4.301	3.806	6.138	3.267	2.2
MnO	0.123	0.097	0.057	0.14	0.153	0.174	0.123
MgO	0.75	1.34	0.85	0.79	1.3	0.64	0.55
CaO	1.32	0.81	1.04	2.29	1.37	1.14	1.57
Na_2O	0.9	3.42	1.28	0.38	1.75	0.2	0.08
K_2O	5.3	3.92	5.61	4.45	4.11	5.19	4.05
P_2O_5	0.134	0.342	0.19	0.162	0.225	0.107	0.083
S	3.13	4.46	2.37	2.16	3.3	1.53	1.06

Sample	PIT-VCV-0002	PIT-VCV-0003	PIT-VCV-0007	PIT-VCV-0008	PIT-VCV-0009	PIT-VCV-0012	PIT-VCV-0013
SO_4	0.05	0.06	0.06	0.04	0.06	0.03	0.04
C	0.29	0.07	0.16	0.67	0.26	0.36	0.37
LOI	4.05	5.09	4.21	4.76	4.9	3.79	3.47
Total	102.16	103.66	101.57	101.49	101.94	100.85	99.65
Ba	886	878	1519	943	971	744	305
Rb	173	130	198	173	168	188	184
Sr	105	164	210	138	171	97	40
Pb	22	27	17	157	25	16	19
Th	12	8	12	11	14	18	18
U	3	2	3	5	3	3	2
Zr	268	166	211	176	194	161	146
Nb	27	10.3	23.9	20.5	20.6	24.9	23.2
Y	58	19	18	13	19	15	11
Sc	6	11	7	5	8	3	3
V	52	93	53	46	71	27	22
Ni	10	10	18	17	9	7	5
Cu	12	6	9	39	5	41	66
Zn	34	62	43	101	78	57	40
Ga	24	20	16	17	17	16	17
Cr	21	44	28	16	41	6	3
Co							
F							
Be							
La	64	48	42	35	41	41	39
Ce	124	94	76	69	77	66	60
Nd	54	40	27	23	29	20	18

Sample	PIT-VCV-0014	PIT-VCV-0017	PIT-VCV-0019	PIT-VCV-0020	PIT-VCV-0021	PIT-VCV-0022	PIT-VCV-0023
description	andesite	andesite	andesite	andesite	andesite	andesite	andesite
SWI	1	1	1	1	1	1	1
SiO_2	73.3	70.05	61.11	60.32	52.11	54.33	51.62
TiO_2	0.3	0.47	0.709	0.75	0.858	0.86	0.838
Al_2O_3	12.35	13.96	18.55	18.5	13.48	12.5	11.98
Fe_2O_3T	2.398	0.408	3.08	4.356	5.874	7.65	8.734
MnO	0.133	0.024	0.025	0.047	0.101	0.075	0.048
MgO	0.58	0.71	0.17	0.33	4.16	3	1.46
CaO	0.96	0.88	2.65	1.89	4.63	4.19	4.51
Na_2O	0.12	0.99	0.31	0.49	2.18	3.28	2.33
K_2O	4.73	7.25	3.68	5.26	3.9	2.77	3.06
P_2O_5	0.088	0.159	0.279	0.296	0.375	0.399	0.421
S	1.08	0.46	0.55	1.44	1.95	4.66	6.33
SO_4	0.04	0.04	1.4	0.1	2.28	1.85	2.04
C	0.29	0.14	0.03	0.05	0.05	0.05	0.06
LOI	3.22	2.48	7.03	5.55	8.36	8.95	10.83
Total	99.59	98.02	99.57	99.38	100.31	104.56	104.26
Ba	746	551	751	999	868	1253	769
Rb	174	206	155	196	165	108	104
Sr	75	169	852	969	489	543	681
Pb	11	18	7	7	6	5	6
Th	18	25	8	7	8	7	8

Sample	PIT-VCV-0014	PIT-VCV-0017	PIT-VCV-0019	PIT-VCV-0020	PIT-VCV-0021	PIT-VCV-0022	PIT-VCV-0023
U	3	3	2	3	3	3	0
Zr	148	222	155	164	166	158	154
Nb	23.7	32.4	8.9	10.8	10.3	10.6	9.9
Y	13	19	16	20	20	18	20
Sc	3	4	19	22	15	14	16
V	23	33	144	130	135	123	126
Ni	5	8	10	19	82	106	26
Cu	3	167	18	18	58	40	27
Zn	35	17	2	4	19	15	7
Ga	17	16	18	19	16	15	15
Cr	5	6	50	74	161	171	170
Co							
F							
Be							
La	41	71	38	38	48	40	38
Ce	66	117	83	82	87	85	
Nd	19	37	37	35	39	39	36

Sample	PIT-VCV-0024	PIT-VCV-0027	PIT-VCV-0029	PIT-VCV-0030	PIT-VTM-0600	ROC-KMD-0001	ROC-KMD-0002
description	andesite	andesite	andesite	andesite	andesite	andesite	andesite
SWI	1	1	1	1	2	2	1
SiO_2	61.86	64.85	63.58	64.81	65.12	61.14	60.4
TiO_2	0.66	0.548	0.544	0.539	0.62	0.7	0.73
Al_2O_3	15.36	15.73	15.8	15.51	14.89	13.61	14.18
Fe_2O_3T	1.529	4.51	4.081	3.784	5.445	5.27	5.654
MnO	0.086	0.019	0.039	0.025	0.098	0.13	0.09
MgO	0.73	1.37	1.54	1.5	2.11	3.11	3.44
CaO	5.22	0.72	1.37	1.15	2.55	2.86	5.26
Na_2O	0.21	1.6	1.67	1.34	3.1	2.84	3.5
K_2O	5.39	4.99	5.6	5.02	3.25	3.23	4.1
P_2O_5	0.534	0.242	0.24	0.246	0.265	0.35	0.35
S	1.01	2.67	2.44	2.48	0.41	0.05	0.02
SO_4	0.13	0.05	0.06	0.04	0.0001	0.01	0.01
C	0.1	0.1	0.25	0.2	0.19	1.74	0.06
LOI	3.81	4.3	4.32	4.99	3.18	6.81	1.38
Total	96.63	101.7	101.53	101.63	101.23	101.85	99.17
Ba	543	1109	1294	1262	1180	1264	1336
Rb	259	158	191	160	119	85	62.5
Sr	98	190	208	211	650	708	1140
Pb	164	12	8	20	21	64	17.3
Th	9	8	8	9	9	8	6.2
U	1	3	2	2	3	2	1
Zr	117	171	170	172	145	209	176.7
Nb	5.4	9.5	9.7	9.5	9	11	9.2
Y	14	14	17	16	13	22	20.1
Sc	11	8	10	7	11	11	13.8
V	83	81	78	85	92	100	110
Ni	24	27	25	24	42	75.5	92.7
Cu	70	20	39	118	164	58	20.5
Zn	247	19	14	18	49	173	71.8

Sample	PIT-VCV-0024	PIT-VCV-0027	PIT-VCV-0029	PIT-VCV-0030	PIT-VTM-0600	ROC-KMD-0001	ROC-KMD-0002
Ga	19	20	19	16	19	20	16.8
Cr	53	39	39	37	72	126	147.6
Co							
F					771	975	
Be							
La	45	39	43	39	34	41	42.6
Ce	68	75	76	74	63	82	86.9
Nd	23	31	31	30	27	37.5	39.3

Sample	ROC-VTM-0032	ROC-VTM-0033	SPR-JWM-0001	SPR-JWM-0002	SPR-VTM-0001	SPR-VTM-0002	SPR-VTM-0007
description	andesite	andesite	andesite	andesite	andesite	andesite	andesite
SWI	2	2	2	2	1	1	2
SiO_2	58.69	60.2	64.59	62.81	61.51	62.97	57.84
TiO_2	0.66	0.78	0.69	0.7	0.705	0.71	0.684
Al_2O_3	16.11	14.92	14.07	14.44	15.415	15.42	15.101
Fe_2O_3T	5.99	5.9	5.346	6.281	5.955	5.78	5.581
MnO	0.1	0.13	0.116	0.109	0.1	0.1	0.236
MgO	1.3	2.1	3.25	3.6	2.51	2.5	3.262
CaO	3.12	3.71	1.77	1.84	3.305	2.7	3.47
Na_2O	2.41	3.48	4.08	4.19	4.7	5.05	2.18
K_2O	3.01	3.68	3.05	2.57	3.175	2.88	3.96
P_2O_5	0.16	0.3	0.298	0.301	0.25	0.25	0.335
S	0	0	0.3	1.11	0.51	0.09	0.0836
SO_4	0	0	0.09	0.04	0.03		
C	0		0.24	0.13	0.28		
LOI	6.49	4.37	2.47	3.1	1.66	0.9	4.93
Total	98.04		100.36	101.22	100.11		
Ba	992	1298	1056	782	1261	1220	1203
Rb	82	87	91	92	93	70	186.5
Sr	594	707	560	553	579	817	495.5
Pb	33.8	31.7	11	8	20.1	21.7	17.5
Th	7.67	7.05	7	6	11.4	8.14	10.5
U	1.31	3.42	3	2	2.785	2.08	3.9
Zr	194	218	165	169	180.5	183	173.9
Nb	12	14	9.3	10.2	12.5	13	10.9
Y	27.7	24	17	17	23.8	21	19.6
Sc			13	13			12.7
V	101	130	93	98	120.5	130	101.2
Ni	4	70	70	80	24.5	10	33.4
Cu	24	40	146	165	158	44	300.7
Zn	81	80	49	44	42	63	43.7
Ga	18.6	18.4	17	21	17.65	17.3	20.6
Cr	52	174	104	101	73.5	77	63.2
Co	45	43			32.5	49	
F	551	755		2415	6853	1171	
Be							
La		51	35	41			48.1
Ce		95	72	79			87.4
Nd		11.7	32	33			37.3

TABLE A1-3. Mineralogy, in weight percent, of relatively unweathered andesites from the Questa-Red River area of samples in Table 1-1 and 1-2, using bulk quantitative mineralogy technique based upon a modified ModAn procedure (McLemore et al., 2009b).

Sample number	110	113	119	78L-187	1830	1831	1832
lithology	hornblende andesite	augite andesite	augite andesite	andesite flow	fresh andesite	fresh andesite	fresh andesite
quartz	15	15	16	11	22	24	23
K-spar/orthoclase	23	29	27	21	17	21	19
plagioclase	18	29	30	34	42	39	34
biotite						4	0.6
magnetite	3		0.1		4	4	4
rutile (sphene)	0.3	0.8	0.8	0.9	0.4	0.2	
apatite	2	1	0.3	1	0.8	0.9	0.9
pyrite					0.01	0.01	0.01
hornblende	4				11	7	18
cpx					2		0.5
actinolite	34			12			
amphibole		26	26	20			

TABLE A1-4. Chemical composition of relatively unweathered quartz latite from the Questa-Red River area from Dillet and Czamanske (1987), Lipman (1988), Johnson et al. (1989), P. Lipman, written communication (2007). Major oxides are in weight percent and trace elements in parts per million (ppm).

Sample	81S-148	PWL	116	22	79L-73
description	Latir latite	latite	Quartz latite	Quartz latite	latite
SiO_2	64.9	65.9	66.8	65.6	63.7
TiO_2	0.64	0.56	0.59	0.6	0.9
Al_2O_3	15.5	15.7	14.7	15.4	15.8
Fe_2O_3T	5.61	4.7	4.82	4.64	5.53
MnO	0.07	0.07	0.09	0.07	0.07
MgO	2.3	2.25	2.31	2.3	2.1
CaO	4.2	4.02	3.99	3.86	4.2
Na_2O	3.6	4.47	3.91	4.08	3.7
K_2O	3.4	2.44	3.03	3.59	3.5
P_2O_5	0.28	0.28	0.27	0.3	0.51
S	0		0	0	0
SO_4	0		0	0	0
C	0		0	0	0
LOI	0.59	3.45	0.48	0.68	0.58
Total	101.09		100.99	101.12	100.59
Ba		1450	1190	1240	
Rb	59	148	53	68	64
Sr	845	840	745	760	1210
Pb		23	22	25	
Th		11	9	10	6
U		4	2	3	2
Zr	131	139	134	134	201
Nb	5	10	9.5	11	20
Y	9	15	12	25	18

Sample	81S-148	PWL	116	22	79L-73
Sc					
V		66	75	73	
Ni		26	29	31	
Cu		22	9	25	
Zn		68	57	63	
Ga					
Cr		42	53	43	
Co					
F					
Be					
La					
Ce		68.07			
Nd		28.91			

TABLE A1-5. Chemical composition of relatively unweathered Amalia Tuff from the Questa-Red River area from Dillet and Czamanske (1987), Lipman (1988), Johnson et al. (1989), P. Lipman, written communication (2007) and this project. Major oxides are in weight percent and trace elements in parts per million (ppm).

Sample	78L-101	78L-115	78L-118	82L-42D	GMG-PIT-0006	GMG-PIT-0007	GMG-PIT-0014	GMG-PIT-0015	PIT-LFG-0009
SiO_2	77.9	79.3	76	78	73.32	73.76	65.82	65.28	74.531
TiO_2	0.14	0.14	0.11	0.11	0.24	0.26	0.53	0.57	0.15
Al_2O_3	12.1	11.8	12.2	11.3	12.07	12.73	15.72	15.11	11.81
Fe_2O_3T	1.12	0.46	2.7	2	0.33	0.77	6.03	3.4	1.945
MnO			0.14	0.05	0.056	0.04	0.01	0.05	0.077
MgO	0.06	0.03	0.16	0	0.24	0.46	0.94	1.43	0.38
CaO	0.21	0	0.43	0.15	1.42	0.91	0.39	1.87	1.033
Na_2O	3.4	3.4	3.3	3.6	1.75	2.16	0.38	0.91	2.008
K_2O	4.9	4.9	4.9	4.7	7.14	5.8	4.92	4.75	4.965
P_2O_5	0.01	0.02	0.05	0	0.058	0.069	0.11	0.11	0.033
S			0	0					0.75
SO_4			0	0					0.05
C	0.04	0.01	0	0					0.25
LOI	0.87	0.59	0.56	0.64	1.55	1.84	5.08	4.54	2.75
Total			100.82	100.75					100.93
Total S	0	0	0	0	0.06	0.05	1.79	0.64	0.8
Ba					448	503	637	1159	143.5
Rb	144	132	125	124	171	161	180	159	148.9
Sr	5	5	28	4	126	115	15	121	68
Pb					14	17	9.3	19	27.5
Th	12.5	10			23	24	12.3	14.49	13.9
U	5.8	5.2			3	6	4.65	3.52	4.9
Zr	309	309	317	310	132	153	204	240	288.5
Nb	39	39	31	37	31	27.7	30	31	34.6
Y	44	44	64	63	11	13	25	18.9	69.5
Sc					2	2			0.4
V					11	15	73	61	7
Ni					8	7	0	0	7
Cu					49	84	7	143	15
Zn	90	30	118		5	15	14	43	59.6
Ga					14	16	17.3	17.2	24.9
Cr					1	3	10	4	6.6
Co							46	27	

Sample	78L-101	78L-115	78L-118	82L-42D	GMG-PIT-0006	GMG-PIT-0007	GMG-PIT-0014	GMG-PIT-0015	PIT-LFG-0009
F	3000	1000			1290	1033	1910	2101	686
Be									
La					53	48			63.8
Ce					82	77			131
Nd					23	24			58

Sample	PIT-RDL-0001	PIT-RDL-0002	PIT-VCV-0004	PIT-VCV-0005	Q82J41P	ROC-MZQ-0004	ROC-NWD-0001	ROC-NWD-0002	ROC-NWD-0003
SiO_2	74.92	78.11	81.8	79.67	77.4	76.29	76.94	60.55	76.46
TiO_2	0.15	0.15	0.135	0.133	0.1	0.1376	0.14	0.82	0.19
Al_2O_3	11.33	11.39	10.45	10.62	12	12.39	12.31	16.78	11.72
Fe_2O_3T	2.1	1.08	0.73	1.33		0.91	0.898	5.84	1.29
MnO	0.02	0.017	0.029	0.034		0.007	0.002	0.065	0.113
MgO	0.35	0.29	0.33	0.36		0.02	0.02	1.73	0.08
CaO	0.05	0.06	0	0	0.09	0.08	0.1	0.52	0.18
Na_2O	0.25	0.39	0.07	0.07	3.9	3.62	3.63	4.91	4.15
K_2O	5.2	5.86	3.46	3.48	5.04	4.83	4.94	3.52	4.79
P_2O_5	0.04	0.024	0.023	0.021		0.009	0.013	0.397	0.015
S	0.02	0.05	0.02	0.02			0	3.5	0.01
SO_4	0.19		0.01	0.23			0.01	0.18	0
C	0.15	0	0.02	0.02			0.04	0.05	0.14
LOI	3.48	1.81	1.99	4.77	0.56	0.79	0.94	4.75	0.52
Total	98.48		99.14	100.89			100.06	104.2	99.79
Total S	0.21	0.05	0.03	0.25			0.01	3.68	0.01
Ba	204	216	75	63		20	17	939	42
Rb	171	191	123	118		136	142	125	110
Sr	60	56	6	3		8	7	268	9
Pb	112	21	107	201		25	32	9	15
Th	12	9	15	13		13	18	7	13
U	8	6	6	4		5	7	3	4
Zr	300.5	310	309	314		385	407	175	348
Nb	35	35.9	34.5	36.3		41	39.8	10.1	31.6
Y	58	59	70	70		65	56	14	57
Sc	1	1	1	1		0	1	13	3
V	11	7	9	6		2		109	10
Ni	5.5	7	1	1		0	6	71	6
Cu	17	7	6	8		0	1	449	4
Zn	32.5	19	16	18		69	58	39	105
Ga	24	25	25	24		25	27	24	22
Cr	9.5	6	4	4		10	2	82	2
Co									
F	848	749					192	1172	332
Be									
La	39	40	65	68		6	5	32	33
Ce	67	85	135	138		6	13	68	79
Nd	26.4	38	56	58		5	6	34	44

TABLE A1-6. Mineralogy, in weight percent, of samples in Table 1-5 of relatively unaltered Amalia Tuff from the Questa-Red River area, using bulk quantitative mineralogy technique based upon a modified ModAn procedure (McLemore et al., 2009b).

Sample	78L-101	78L-115	78L-118	82L-42D	GMG-PIT-0006	GMG-PIT-0007	GMG-PIT-0014	GMG-PIT-0015	PIT-LFG-0009	PIT-RDL-0001
quartz	41	43	38.6	43	36	38	33	32	42	48
K-spar/orthoclase	39	39	39.5	36	58	44	23	28	34	31
plagioclase	19	18	18.5	19	0.8	8		1	8	
illite					2	7	33	23	8	16
chlorite						1	2	4	1	
smectite							1	1	1	0.8
kaolinte									1	
epidote							0.8	9		
Fe oxides	1	0.5	3.5	2	0.4	0.5	5	0.1	1	2
rutile (sphene)	0.1	0.1			0.2	0.2	0.3	0.6	0.1	0.1
apatite				0.1	1	0.9	0.3	0.3		
pyrite					0.1	0.1	3	1	1	0.01
calcite	0.3			0.1	0.9	0.5			2	1
gyp									0.2	0.02
zircon	0.06	0.06		0.06	0.03	0.03	0.04	0.04	0.06	0.06
fluorite									0.02	
jarosite									0.03	1
chalcopyrite										
TOTAL	100.46	100.66	100.1	100.26	99.43	100.23	101.44	100.04	99.41	99.99

Sample	PIT-RDL-0002	PIT-VCV-0004	PIT-VCV-0005	Q82J41P	ROC-MZQ-0004	ROC-NWD-0001	ROC-NWD-0002	ROC-NWD-0003
quartz	46	59	57	40.1	57	39	16	40
K-spar/orthoclase	40	16	16	38.5	16	39	20	36
plagioclase				19.7		20	36	21
illite	10	21	22		22		10	
chlorite	0.6	1	1		1		5	
smectite	1	1	1		1		3	
kaolinte	1	1	1		1		1	
epidote								
Fe oxides	1	1	1	1.5	1	1	0.8	2
rutile (sphene)	0.1	0.1	0.1		0.1	0.1	0.8	0.1
apatite	0.1	0.01	0.01		0.01	0.01	0.6	0.01
pyrite	0.1	0.01	0.01		0.01	0.01	6	0.01
calcite		0.1	0.1		0.1	0.2	0.2	0.8
gyp						0.05	0.2	
zircon	0.06	0.06	0.06		0.07	0.07	0.03	0.07
fluorite								
jarosite							0.7	
chalcopyrite							0.01	
TOTAL	99.96	100.28		99.8	99.29	99.44	100.34	99.99

TABLE A1-7. Chemical composition of relatively unaltered Goat Hill Porphyry from the Questa-Red River area (from Dillet and Czamanske, 1987; Lipman, 1988; Johnson et al., 1989; P. Lipman, written communication, 2007). Major oxides are in weight percent and trace elements in parts per million (ppm).

Sample	79L-1A	79L-2
lithology	Goat Hill, lithic-rich tuff	Goat Hill, welded-tuff
SiO_2	82	70.6
TiO_2	0.3	0.38
Al_2O_3	11.8	13.4
Fe_2O_3T	1.21	4.95
FeOT	1.1	4.5
MnO	0.06	0.31
MgO	0.61	1.6
CaO	0.02	2.2
Na_2O	0.15	2.8
K_2O	3.8	4.2
P_2O_5	0.05	0.16
LOI	1.8	2.6
Total	101.8	103.2
Rb	157	117
Sr	5	213
Zr	127	202
Nb	20	27
Y	9	42
Zn	38	130

TABLE A1-8. Chemical composition of relatively unweathered granitic intrusions from the Questa-Red River area obtained from this study. Major oxides are in weight percent and trace elements in parts per million (ppm).

Sample	MIN-DCS-0001	GHN-ACT-0036	GHN-VTM-0500	GHN-VTM-0503	GHN-VTM-0624	MIN-VTM-0020	MIN-VTM-0021	PIT-VTM-0004
SiO_2	64.32	64.03	62.08	58.87	62.55	62.3	62.35	63.422
TiO_2	0.65	0.57	0.56	0.56	0.68	0.64	0.62	0.61
Al_2O_3	14.16	15.49	15.45	16.55	15.68	15.5	16.37	14.76
Fe_2O_3T	3.245	5.126	4.97	4.34	4.93	5.43	5.918	5.5077
FeOT	2.95	4.66				4.89	5.38	5.007
MnO	0.08	0.021	0.3	0.38	0.08	0.15	0.07	0.0576
MgO	2.21	1.2	3.7	2.46	1.56	1.46	1.67	2.861
CaO	2.47	0.07	2.18	2.32	0.6	0.53	0.41	2.624
Na_2O	1.85	1.14	1.08	1.69	0.77	0.95	0.15	2.325
K_2O	5.26	3.31	3.31	3.16	3.61	3.7	3.98	2.676
P_2O_5	0.29	0.143	0.19	0.17	0.21	0.32	0.28	0.262
S	0.83		0.08	0	0.03	0.04	0.03	1
SO4	0.1		0.14	1.13	0.58	0.04	0.02	
C	0.31	0	0.48	0.13	0.62	0.78	0.19	
LOI	3.01	6.7	5.31	7.14	8.36	7.14	5.53	4.69
Ba	863	1323	1117	915	797	1218	947.7	881.5
Rb	232	101	90	80	87	102	112.4	124

Sample	MIN-DCS-0001	GHN-ACT-0036	GHN-VTM-0500	GHN-VTM-0503	GHN-VTM-0624	MIN-VTM-0020	MIN-VTM-0021	PIT-VTM-0004
Sr	367	172	181	161	101	174	65.2	495.8
Pb	122	22	9	10	63	33	96	21.1
Th	13	10	6	4	7	6	6.4	7.2
U	1	3	2	2	3	5	2.7	3.7
Zr	153	160	145	139	168	207	162.9	151.3
Nb	13.5	9.1	8.1	7.1	10	11	8.3	9.6
Y	19	35	34	24	26	22	18.3	16.1
Sc	12	9	10	10	9	9	10.7	9.8
V	105	87	82	80	85	80	88	90
Ni	42	33	53	75	35	57	62.3	36.8
Cu	165	15	46	65	34	44	29.2	69.5
Zn	240	130	304	537	266	159	256.8	52.8
Ga	18	19	18	19	18	18	20.4	19.8
Cr	77	59	43	40	42	67	78.1	71.5
F		865	1050	1166	1068	1149		1367
La	45	38	41	29	35	43	26	36.3
Ce	82	74	67	73	68	84	56.5	62.7
Nd	32	31	43	36	34	37	28.4	25.9

Sample	PIT-VWL-0001	SGS-RDL-0002	SMM-VWL-0002	SSS-RDL-0006	GHN-VTM-0510	PIT-VTM-0010	GMG-PIT-0001	GMG-PIT-0007
SiO_2	76.79	63.69	63.96	60.88	55.29	60.66	53.65	73.76
TiO_2	0.14	0.6	0.54	0.73	0.57	0.68	0.97	0.26
Al_2O_3	10.25	13.47	14.46	14.19	17.8	15.02	20.96	12.73
Fe_2O_3T	2.19	3.795	4.51	5.434	5.661	7	5.45	0.847
FeOT		3.45	4.1	4.94				0.77
MnO	0.01	0.096	0.067	0.282	0.06	0.08	0.05	0.04
MgO	0.23	2.63	1.78	3.23	1.62	2.26	0.28	0.46
CaO	0.03	2.48	2.85	3.17	0.37	1.6	3.66	0.91
Na_2O	0.66	2.15	3.09	2.78	2.08	2.2	0.34	2.16
K_2O	5.69	4.13	2.79	3.86	3.75	3.43	5.3	5.8
P_2O_5	0	0.286	0.239	0.332	0.25	0.27	0.15	0.069
S	0.62	0.15	0.028	0.2085		1.2		
SO4								
C					0			
LOI	3.18	0.67	4.63	3.52	9.31	5.35	5.19	1.84
Ba	160	1426	1169	915	2863	1250	862	503
Rb	170	157	58	154	95	123	199	161
Sr	29	374	424	488	437	502	1004	115
Pb	60.4	85	27	109	38	52	13	17
Th	11.22	8	7	10	10	8.45	6.76	24
U	5.25	2	2.5	4	3	2	0.3	6
Zr	341	157	133	169	144	144	222	153
Nb	41	9.4	10	13.1	8.1	11	16	27.7
Y	58.9	15	19	19	22	13.5	28.3	13
Sc		10	8	13	10	11		2
V	0	92	88	108	100	118	189	15
Ni	0	47	32	61	38	31	22	7
Cu	12	96	27	98	19	118	40	84
Zn	10	68	90	246	156	57	6	15

Sample	PIT-VWL-0001	SGS-RDL-0002	SMM-VWL-0002	SSS-RDL-0006	GHN-VTM-0510	PIT-VTM-0010	GMG-PIT-0001	GMG-PIT-0007
Ga	18.8	16	18	20	24	19	17.5	16
Cr	11	72	58	147	53	98	61	3
F					1372	1198		
La		43	36	45	40	35		48
Ce		80	76	91	69	67		77
Nd		35	32	38	35	29.5		24

Sample	PIT-KMD-0009	PIT-VCV-0001	PIT-VCV-0002	PIT-VCV-0003	PIT-VCV-0007	PIT-VCV-0008	PIT-VCV-0009	PIT-VCV-0012
SiO_2	63.74	62.64	68.37	61.44	66	68.84	63.49	71.65
TiO_2	0.65	0.686	0.352	0.708	0.56	0.443	0.591	0.324
Al_2O_3	14.98	15.49	13.16	16.07	14.88	12.56	14.29	12.45
Fe_2O_3T	4.1	5.346	4.235	5.83	4.301	3.806	6.138	3.267
FeOT		4.86	3.85	5.3	3.91	3.46	5.58	2.97
MnO	0.1	0.134	0.123	0.097	0.057	0.14	0.153	0.174
MgO	2.39	0.9	0.75	1.34	0.85	0.79	1.3	0.64
CaO	3.37	1.02	1.32	0.81	1.04	2.29	1.37	1.14
Na_2O	3.35	2.62	0.9	3.42	1.28	0.38	1.75	0.2
K_2O	4.06	4.75	5.3	3.92	5.61	4.45	4.11	5.19
P_2O_5	0.24	0.337	0.134	0.342	0.19	0.162	0.225	0.107
S	0.25	4.43	3.13	4.46	2.37	2.16	3.3	1.53
SO4		0.05	0.05	0.06	0.06	0.04	0.06	0.03
C		0.15	0.29	0.07	0.16	0.67	0.26	0.36
LOI	3	4.91	4.05	5.09	4.21	4.76	4.9	3.79
Ba	1237	1054	886	878	1519	943	971	744
Rb	121	151	173	130	198	173	168	188
Sr	637	165	105	164	210	138	171	97
Pb	26.3	31	22	27	17	157	25	16
Th	6.97	10	12	8	12	11	14	18
U	1.77	3	3	2	3	5	3	3
Zr	145	171	268	166	211	176	194	161
Nb	14	12.2	27	10.3	23.9	20.5	20.6	24.9
Y	15.5	19	58	19	18	13	19	15
Sc		11	6	11	7	5	8	3
V	102	103	52	93	53	46	71	27
Ni	0	10	10	10	18	17	9	7
Cu	23	20	12	6	9	39	5	41
Zn	67	41	34	62	43	101	78	57
Ga	17.8	21	24	20	16	17	17	16
Cr	76	44	21	44	28	16	41	6
F	2865							
La		38	64	48	42	35	41	41
Ce		78	124	94	76	69	77	66
Nd		34	54	40	27	23	29	20

Sample	PIT-VCV-0013	PIT-VCV-0014	PIT-VCV-0017	PIT-VCV-0019	PIT-VCV-0020	PIT-VCV-0021	PIT-VCV-0022	PIT-VCV-0023
SiO_2	73.97	73.3	70.05	61.11	60.32	52.11	54.33	51.62
TiO_2	0.278	0.3	0.47	0.709	0.75	0.858	0.86	0.838
Al_2O_3	11.81	12.35	13.96	18.55	18.5	13.48	12.5	11.98
Fe_2O_3T	2.2	2.398	0.408	3.08	4.356	5.874	7.65	8.734
FeOT	2	2.18	1.02	2.8	3.96	5.34	6.96	7.94

Sample	PIT-VCV-0013	PIT-VCV-0014	PIT-VCV-0017	PIT-VCV-0019	PIT-VCV-0020	PIT-VCV-0021	PIT-VCV-0022	PIT-VCV-0023
MnO	0.123	0.133	0.024	0.025	0.047	0.101	0.075	0.048
MgO	0.55	0.58	0.71	0.17	0.33	4.16	3	1.46
CaO	1.57	0.96	0.88	2.65	1.89	4.63	4.19	4.51
Na_2O	0.08	0.12	0.99	0.31	0.49	2.18	3.28	2.33
K_2O	4.05	4.73	7.25	3.68	5.26	3.9	2.77	3.06
P_2O_5	0.083	0.088	0.159	0.279	0.296	0.375	0.399	0.421
S	1.06	1.08	0.46	0.55	1.44	1.95	4.66	6.33
SO4	0.04	0.04	0.04	1.4	0.1	2.28	1.85	2.04
C	0.37	0.29	0.14	0.03	0.05	0.05	0.05	0.06
LOI	3.47	3.22	2.48	7.03	5.55	8.36	8.95	10.83
Ba	305	746	551	751	999	868	1253	769
Rb	184	174	206	155	196	165	108	104
Sr	40	75	169	852	969	489	543	681
Pb	19	11	18	7	7	6	5	6
Th	18	18	25	8	7	8	7	8
U	2	3	3	2	3	3	3	0
Zr	146	148	222	155	164	166	158	154
Nb	23.2	23.7	32.4	8.9	10.8	10.3	10.6	9.9
Y	11	13	19	16	20	20	18	20
Sc	3	3	4	19	22	15	14	16
V	22	23	33	144	130	135	123	126
Ni	5	5	8	10	19	82	106	26
Cu	66	3	167	18	18	58	40	27
Zn	40	35	17	2	4	19	15	7
Ga	17	17	16	18	19	16	15	15
Cr	3	5	6	50	74	161	171	170
F								
La	39	41	71	38	38	48	40	38
Ce	60	66	117	83	82	87	85	
Nd	18	19	37	37	35	39	39	36

Sample	PIT-VCV-0024	PIT-VCV-0027	PIT-VCV-0029	PIT-VCV-0030	PIT-KMD-0008	PIT-KMD-0007	average	standard deviation
SiO_2	61.86	64.85	63.58	64.81	63.96	63.27	63.8	5.8
TiO_2	0.66	0.548	0.544	0.539	0.61	0.59	0.6	0.2
Al_2O_3	15.36	15.73	15.8	15.51	14.69	14.32	14.2	2.1
Fe_2O_3T	1.529	4.51	4.081	3.784	3.92	2.5	2.9	1.8
FeOT	1.39	4.1	3.71	3.44			3.0	1.7
MnO	0.086	0.019	0.039	0.025	0.07	0.11	0.1	0.1
MgO	0.73	1.37	1.54	1.5	1.79	2.39	2.3	1.0
CaO	5.22	0.72	1.37	1.15	1.71	2.85	2.7	1.3
Na_2O	0.21	1.6	1.67	1.34	3.89	3.26	2.6	1.1
K_2O	5.39	4.99	5.6	5.02	2.89	5.76	5.5	1.1
P_2O_5	0.534	0.242	0.24	0.246	0.04	0.18	0.2	0.1
S	1.01	2.67	2.44	2.48	1.61	1.97	1.4	1.6
SO4	0.13	0.05	0.06	0.04			0.1	0.7
C	0.1	0.1	0.25	0.2			0.3	0.2
LOI	3.81	4.3	4.32	4.99	4.17	2.44	2.7	2.2
Ba	543	1109	1294	1262	1404	1333	1098	434
Rb	259	158	191	160	130	186	209	45
Sr	98	190	208	211	282	496	432	256

Sample	PIT-VCV-0024	PIT-VCV-0027	PIT-VCV-0029	PIT-VCV-0030	PIT-KMD-0008	PIT-KMD-0007	average	standard deviation
Pb	164	12	8	20	46.1	44.2	83	41
Th	9	8	8	9	5.29	7.52	10	5
U	1	3	2	2	1.79	0.97	1	1
Zr	117	171	170	172	228	176	165	41
Nb	5.4	9.5	9.7	9.5	15	11	12	8
Y	14	14	17	16	22.5	17.2	18	10
Sc	11	8	10	7			12	4
V	83	81	78	85	161	116	111	41
Ni	24	27	25	24	100	12	27	27
Cu	70	20	39	118	175	295	230	61
Zn	247	19	14	18	119	67	154	114
Ga	19	20	19	16	20.6	16.6	17	2
Cr	53	39	39	37	401	89	83	71
F					6004	3515	3515	1580
La	45	39	43	39			45	8
Ce	68	75	76	74			82	14
Nd	23	31	31	30			32	7